Simulating Coupled Surface-Subsurface Flows with ParFlow v3.5.0: Capabilities, applications, and ongoing development of an open-source, massively parallel, integrated hydrologic model

Benjamin N. O. Kuffour[1,*], Nicholas B. Engdahl[1], Carol S. Woodward[2],

Laura E. Condon[3], Stefan Kollet[4,5], and Reed M. Maxwell[6]

[1]Civil and Environmental Engineering, Washington State University, Pullman, WA, USA

[2]Center for Applied Scientific Computing, Lawrence Livermore National Laboratory, Livermore, CA, USA

[3]Hydrology and Atmospheric Sciences, University of Arizona, Tucson, AZ, USA

[4]Institute for Bio- and Geosciences, Agrosphere (IBG-3), Research Centre Jülich, Geoverbund ABC/J, Jülich

[5]Centre for High-Performance Scientific Computing in Terrestrial Systems, Geoverbund ABC/J, Jülich

[6]Integrated GroundWater Modeling Center and Department of Geology and Geological Engineering, Colorado School of Mines, Golden, CO, USA

Correspondence to: Benjamin N. O. Kuffour (b.kuffour@wsu.edu)

i

27   Abstract

28   Surface and subsurface flow constitute a naturally linked hydrologic continuum that has not

29   traditionally been simulated in an integrated fashion. Recognizing the interactions between these

30   systems has encouraged the development of integrated hydrologic models (IHMs) capable of

31   treating surface and subsurface systems as a single integrated resource. IHMs is dynamically

32   evolving with improvement in technology and the extent of their current capabilities are often only

33   known to the developers and not general users. This article provides an overview of the core

34   functionality, capability, applications, and ongoing development of one open-source IHM,

35   ParFlow. ParFlow is a parallel, integrated, hydrologic model that simulates surface and subsurface

36   flows. ParFlow solves Richards' equation for three-dimensional variably saturated groundwater

37   flow and the two-dimensional kinematic wave approximation of the shallow water equations for

38   overland flow. The model employs a conservative centered finite difference scheme and a

39   conservative finite volume method for subsurface flow and transport, respectively. ParFlow uses

40   multigrid preconditioned Krylov and Newton-Krylov methods to solve the linear and nonlinear

41   systems within each time step of the flow simulations. The code has demonstrated very efficient

42   parallel solution capabilities. ParFlow has been coupled to geochemical reaction, land surface

43   (e.g. Common Land Model), and atmospheric models to study the interactions among the

44   subsurface, land surface, and the atmosphere systems across different spatial scales. This overview

45   focuses on the current capabilities of the code, the core simulation engine, and the primary

46   couplings of the subsurface model to other codes, taking a high-level perspective.

1. Introduction

Surface and subsurface (unsaturated and saturated zones) water are connected components of a hydrologic continuum (Kumar et al., 2009) . The recognition that flow systems (i.e. surface and subsurface) are a single integrated resource has stimulated the development of integrated hydrologic models (IHMs), which include codes like ParFlow (Ashby and Falgout, 1996; Kollet and Maxwell, 2006) , HydroGeoSphere (Therrien and Sudicky, 1996), PIHM (Kumar, 2009), and CATHY (Camporese et al., 2010) . These codes explicitly simulate different hydrological processes such as feedbacks between processes that affect the timing and rates of evapotranspiration, vadose zone flow, surface runoff and groundwater interactions. That is, IHMs are designed specifically to include the interactions between traditionally incompatible flow domains (e.g. groundwater and land surface flow) (Engdahl and Maxwell, 2015) . Most IHMs adopt a similar, physically-based approach to describe watershed dynamics where the governing equations of three–dimensional variably saturated subsurface flow are coupled to shallow water equations for surface runoff. The advantage of the coupled approach is that it allows hydraulically-connected groundwater–surface water systems to evolve dynamically, and for natural feedbacks between the systems to develop (Sulis et al., 2010; Maxwell et al., 2011; Weill et al., 2011; Williams and Maxwell, 2011; Simmer et al., 2015). A large body of literature now exists presenting applications of the various IHMs to solve hydrologic questions. Each model has its own technical documentation, but the individual development, maintenance, and sustainability efforts differ between tools. Some IHMs represent commercial investments and others are community,

69 open-sourced projects, but all are dynamically evolving as technology improves and new features

70 are added. Consequently, it can be difficult to answer the question of "what exactly can this IHM

71 do today" without navigating dense user documentation. The purpose of this manuscript is to

72 provide a current review of the functions, capabilities, and ongoing development of one of the

73 open-source integrated models, ParFlow, in a format that is more accessible to a broad audience

74 than a user manual or articles detailing specific applications of the model.

75 ParFlow is a parallel integrated hydrologic model that simulates surface and groundwater flow

76 (Maxwell et al., 2016). ParFlow computes fluxes through the subsurface, as well as interactions

77 with aboveground or surface (overland) flow: all driven by gradients in hydraulic head. Richards'

78 equation is employed to simulate variably saturated three-dimensional groundwater flow

79 (Richards, 1931). Overland flow can be generated by saturation or infiltration excess using a free

80 overland flow boundary condition combined with Manning's equation and the kinematic wave

81 formulations of the dynamic wave equation (Kollet and Maxwell, 2006). ParFlow solves these

82 governing equations employing either a fully coupled or integrated approach where surface and

83 subsurface flows are solved simultaneously the Richards' equation in three-dimensional form

84 (Gilbert and Maxwell, 2016) , or an indirect approach where the different components can be

85 partitioned and flows in only one of the systems (surface or subsurface flows) is solved. The

86 integrated approach allows for dynamic evolution of the interconnectivity between the surface

87 water and groundwater systems. This interconnection depends only on the properties of the

88 physical system and governing equations. An indirect approach permits partitioning of the flow

89 components i.e. water and mass fluxes between surface and subsurface systems. The flow

components can be solved sequentially. For the groundwater flow solution, ParFlow makes use of an implicit backward Euler scheme in time, and a cell-centered finite-difference scheme in space (Woodward, 1998). An upwind finite-volume scheme in space and an implicit backward Euler scheme in time is used for the overland flow component (Maxwell et al., 2007). ParFlow uses Krylov linear solvers with multigrid preconditioners for the flow equations along with a Newton method for the nonlinearities in the variably saturated flow system (Ashby and Falgout, 1996; Jones and Woodward, 2001). ParFlow's physically based approach requires a number of parameterizations e.g. subsurface hydraulic properties, such as porosity, the saturated hydraulic conductivity, and the pressure-saturation relationship parameters (relative permeability), etc. (Kollet and Maxwell, 2008a).

ParFlow is well documented and has been applied to surface and subsurface flow problems including simulating the dynamic nature of groundwater and surface-subsurface interconnectivity in large domains (e.g. over 600 km^2) (Kollet and Maxwell, 2008; Ferguson and Maxwell, 2012; Condon et al., 2013; Condon and Maxwell, 2014), small catchments (e.g. approximately 30 km^2) (Ashby et al., 1994; Kollet and Maxwell, 2006; Engdahl et al., 2016), complex terrain with highly heterogenous subsurface permeability such as the Rocky Mountain National Park, Colorado, United States (Engdahl and Maxwell, 2015; Kollet et al., 2017), large watersheds (Abu-El-Sha'r and Rihani, 2007; Kollet et al., 2010), continental scale flows (Condon et al., 2015; Maxwell et al., 2015) and even subsurface–surface and –atmospheric coupling (Maxwell et al., 2011; Williams and Maxwell, 2011; Williams et al., 2013; Gasper et al., 2014; Shrestha et al., 2015). Evidences from these studies suggest ParFlow produce accurate results in simulating flows in

111 surface-subsurface systems in watersheds i.e. the code possesses the capability of performing

112 simulations that accurately represent the behaviors of natural systems on which models are based.

113 The rest of the paper is organized as follows: We provide a brief history of ParFlow's development

114 in Section 1.1. In Section 2, we describe the core functionality of the code, i.e. the primary

115 functions and the model equations and grid type used by ParFlow. Section 3 covers equation

116 discretization and solvers (e.g. inexact Newton-Krylov, the ParFlow Multigrid (PFMG)

117 preconditioner, and the Multigrid-Preconditioned Conjugate Gradient (MGCG) method) used in

118 ParFlow. Examples of parallel scaling and performance efficiency of ParFlow are revisited in

119 Section 4. The coupling capabilities of ParFlow, with other atmospheric, land surface, and

120 subsurface models are shown in Section 5. We provide a summary and discussion, future directions

121 to the development of ParFlow, and give some concluding remarks in Section 6.

122 1.1 Development History

123 ParFlow development commenced as part of an effort to develop an open–source, object–

124 oriented, parallel watershed flow model initiated by scientists from the Center for Applied

125 Scientific Computing (CASC), Environmental Programs, and the Environmental Protection

126 Department at the Lawrence Livermore National Laboratory (LLNL) in the mid–1990s. ParFlow

127 was born out of this effort to address the need for a code that combines fast, nonlinear solution

128 schemes with massively parallel processing power, and its development continues today (e.g.

129 Ashby et al., 1993; Smith et al., 1995; Woodward, 1998; Maxwell and Miller, 2005; Kollet and

130 Maxwell, 2008; Rihani et al., 2010; Simmer et al., 2015). ParFlow, is now a collaborative effort

131 between numerous institutions including Colorado School of Mines, Research Center Jülich,

132 University of Bonn, Washington State University, the University of Arizona, and Lawrence

133 Livermore National Laboratory, and its working base and development community continues to

134 expand.

135   ParFlow was originally developed for modeling saturated fluid flow and chemical transport

136 in three-dimensional heterogeneous media. Over the past few decades, ParFlow underwent several

137 modifications and expansions (i.e. additional features and capabilities have been implemented)

138 and has seen an exponential growth of applications. For example, a two-dimensional distributed

139 overland flow simulator (surface water component) was implemented into ParFlow (Kollet and

140 Maxwell, 2006) to simulate interaction between surface and subsurface flows. Such additional

141 implementations have resulted in improved numerical methods in the code. The code's

142 applicability continues to evolve, for example, in recent times, ParFlow has been used in several

143 coupling studies, with subsurface, land surface, and atmospheric models to include physical

144 processes at the land surface (Maxwell and Miller, 2005; Maxwell et al., 2007, 2011; Kollet, 2009;

145 Williams and Maxwell, 2011; Valcke et al., 2012; Valcke, 2013; Shrestha et al., 2014; Beisman et

146 al., 2015) across different spatial scales and resolutions (Kollet and Maxwell, 2008; Condon and

147 Maxwell, 2015; Maxwell et al., 2015). Also, a terrain following mesh formulation has been

148 implemented (Maxwell, 2013) that allows ParFlow to handle problems with fine space

149 discretization near the ground surface that comes with variable vertical discretization flexibility

150   which offer modelers the advantage to increase the resolution of the shallow soil layers (these are

151   discussed in detail below).

152

153   2. Core Functionality of ParFlow

154   The core functionality of the ParFlow model is the solution of three-dimensional variably

155   saturated groundwater flow in heterogeneous porous media ranging from simple domains with

156   minimal topography and/or heterogeneity to highly resolved continental-scale catchments (Jones

157   and Woodward, 2001; Maxwell and Miller, 2005; Kollet and Maxwell, 2008; Maxwell, 2013).

158   Within this range of complexity, the ParFlow model can operate in three different modes: 1).

159   variably saturated; 2). steady–state saturated; and 3). integrated–watershed flows; however, all

160   these modes share a common sparse coefficient matrix solution framework.

161   2.1 Variably Saturated Flow

162   ParFlow can operate in variably saturated mode using the well-known, mixed form of

163   Richards' equation (Celia et al., 1990). The mixed form of Richards' equation implemented in

164   ParFlow is:

165    $$S_s S_w(p) \frac{\partial p}{\partial t} + \phi \frac{\partial (S_w(p))}{\partial t} = \nabla . \boldsymbol{q} + q_s, \qquad (1)$$

166    $$\boldsymbol{q} = -k_s k_r(p) \nabla (p - z), \qquad (2)$$

167   where S_s is the specific storage coefficient [L^{-1}], S_w is the relative saturation [$-$] as a function of

168   pressure head p of the fluid/water [L], t is time [T], ϕ is the porosity of the medium [$-$], $\boldsymbol{q}$ is the

169   specific volumetric (Darcy) flux $[LT^{-1}]$, k_s is the saturated hydraulic conductivity tensor $[LT^{-1}]$,

170   k_r is the relative permeability $[-]$ which is a function of pressure head, q_s is the general source/sink

171   term $[T^{-1}]$ (includes wells and surface fluxes e.g. evaporation and transpiration), and z is depth

172   below the surface $[L]$. The Richards' equation assumes that the air phase is infinitely mobile

173   (Richards, 1931). ParFlow has been used to numerically simulate river-aquifer exchange (free-

174   surface flow and subsurface flow), (Frei et al., 2009), and highly heterogenous problems under

175   variably-saturated flow conditions (Woodward, 1998; Jones and Woodward, 2001; Kollet et al.,

176   2010). Under saturated conditions e.g. simulating linear groundwater movement under assumed

177   predevelopment conditions, the steady-state saturated mode can be used.

178

179   2.2 Steady–State Saturated Flow

180   The most basic operational mode is the solution of the steady state, fully saturated

181   groundwater flow equation:

182 $$\nabla . \boldsymbol{q} - q_s = 0, \tag{3}$$

183   where q_s represents a general source/sink term e.g. wells $[T^{-1}]$, $\boldsymbol{q}$ is the Darcy' flux $[L\ T^{-1}]$

184   which is usually written as:

185 $$\boldsymbol{q} = -k_s \nabla P \tag{4}$$

186   where k_s is the saturated hydraulic conductivity $[LT^{-1}]$ and P represents the 3-D hydraulic head-

187   potential $[L]$. ParFlow does include a direct solution option for the steady state saturated flow that

188   is distinct from the transient solver. For example, ParFlow uses the solver "impes" under single-

189   phase, fully saturated steady state condition relative to the variably saturated, transient mode where

190   Richards' equation solver is used (Maxwell et al., 2016). When studying sophisticated or complex

191   phenomena e.g. simulating fully coupled system (i.e. surface and subsurface flow), an overland

192   flow boundary condition is employed.

193

194   2.3 Overland Flow

195   Surface water systems are connected to the subsurface, and these interactions are

196   particularly important for rivers. However, these connections have been historically difficult to

197   represent explicitly in numerical simulations. A common approach has been to use river routing

198   codes, like HEC, and MODFLOW and its River Package to determine head in the river, which is

199   then used as a boundary condition for the subsurface model. This approach prevents feedbacks

200   between the two models, and a better representation of the physical processes in these kinds of

201   problems is one of the motivations for IHMs. Overland flow is implemented in ParFlow as a two–

202   dimensional kinematic wave equation approximation of the shallow water equations. The

203   continuity equation for two-dimensional shallow overland flow is given as;

204    $$\frac{\partial \psi_s}{\partial t} = \nabla . (\vec{v}\psi_s) + q_s,$$ (5)

205   where $\vec{v}$ is the depth averaged velocity vector $[LT^{-1}]$, ψ_s is the surface ponding depth $[L]$, t is time

206    $[T]$, and q_s is a general source/sink (e.g. precipitation rate) $[T^{-1}]$. Ignoring the dynamic and

207   diffusion terms results in the momentum equation

208    $$S_{f,i} = S_{o,i},$$ (6)

209   which is known as the kinematic wave approximation. The $S_{f,i}$ and $S_{o,i}$ represent the friction $[-]$

210   and bed slopes (gravity forcing term) $[-]$ respectively, where i indicates $x-$ and $y-$ directions

211   (also shown in equations 7 and 8) (Maxwell et al., 2015). Manning's equation is used to generate

212   a flow depth–discharge relationship:

213 $$v_x = \frac{\sqrt{S_{f,x}}}{n} \psi_s^{2/3}, \text{ and} \tag{7}$$

214 $$v_y = \frac{\sqrt{S_{f,y}}}{n} \psi_s^{2/3} \tag{8}$$

215   where n is the Manning's roughness coefficient $[\text{TL}^{-1/3}]$. Flow of water out of overland flow

216   simulation domain only occurs horizontally at an outlet which is controlled by specifying a type

217   of boundary condition at the edge of the simulation domain. In a natural system, the outlet is

218   usually taken as the region where a river enters another water body such as stream or a lake.

219   ParFlow determines overland flow direction through the D4 flow routing approach. In a simulation

220   domain, the D4 flow routing approach allows for flow to be assigned from a focal cell to only one

221   neighboring cell accessed via the steepest or most vertical slope. The shallow overland flow

222   formulation (equation 9) assumes that the flow depth is averaged-vertically and neglects a vertical

223   change in momentum in the column of surface water. To account for vertical flow (from the surface

224   to the subsurface or subsurface to the surface), a formulation that couples the system of equations

225   through a boundary condition at the land surface becomes necessary. Equation (5) can be modified

226   to include an exchange rate with the subsurface, q_e, as:

227 $$\frac{\partial \psi_s}{\partial t} = \nabla . (\vec{v} \psi_s) + q_s + q_e \tag{9}$$

228   which is common in other IHMs. In ParFlow, the overland flow equations are coupled directly to

229   Richards' equation at the top boundary cell under saturated conditions. Conditions of continuity

230   of pressure (i.e. the pressures of the subsurface and surface domains are equal right at the ground

231   surface) and flux at the top cell of the boundary between the subsurface and surface systems are

232   assigned Figure 1 is provided demonstrating continuity of pressure at the ground surface for flow

233   from the surface into the subsurface. This assignment is done by setting pressure–head, in equation

234   (1) equal to the vertically–averaged surface pressure, ψ_s;

235    $$p = \psi_s = \psi, \tag{10}$$

236   and the flux, q_e equal to the specified boundary conditions (e.g. Neumann or Dirichlet type). For

237   example, if Neumann type boundary conditions are specified, which are given as;

238    $$q_{BC} = -k_s k_r \nabla(\psi - z) \tag{11}$$

239   and one solves for the flux term in equation (10), the result is;

240    $$q_e = \frac{\partial \|\psi, 0\|}{\partial t} - \nabla \vec{v} \|\psi, 0\| - q_s \tag{12}$$

241   where the $\|\psi, 0\|$ operator is defined as the greater of the quantities, ψ and 0. Substituting equation

242   (12) for the boundary condition in equation (11), requiring the aforementioned flux continuity

243    $q_{BC} = q_e$, leads to

244    $$-k_s k_r \nabla(\psi - z) = \frac{\partial \|\psi, 0\|}{\partial t} - \nabla \cdot (\vec{v} \|\psi, 0\|) - q_s \tag{13}$$

245   Equation (13) shows that the surface water equations are represented as a boundary condition to

246   the Richards' equation. That is, the boundary condition links flow processes in the subsurface with

247   those at the land surface. This boundary condition eliminates the exchange flux and accounts for

248   the movement of the free surface of ponded water at the land surface (Kollet and Maxwell, 2006;

249   Williams and Maxwell, 2011).

250   Many IHMs couple subsurface and surface flows making use of the exchange flux, q_e

251   model. The exchange flux between the domains (the surface and the subsurface) depends on

252   hydraulic conductivity and the gradient across some interface where indirect coupling is used

253   (VanderKwaak, 1999; Panday and Huyakorn, 2004). The exchange flux concept gives a general

254   formulation of a single set of coupled surface-subsurface equations. The exchange flux term, q_e

255   may be included in the shallow overland flow continuity equation as the exchange rate term with

256   the subsurface (equation 9) in a coupled system (Kollet and Maxwell, 2006).

257   Figure. 1 Caption: Coupled surface and subsurface flow systems. Note in this figure the physical

258   system is represented on the left and a schematic of the overland flow boundary condition

259   (continuity of pressure and flux at the ground surface) is on the right. The equation, $p = \psi_s = \psi$

260   in Figure. 1 signifies that the vertically averaged surface pressure and subsurface pressure head are

261   equal right at the land surface.

262

263   2.4 Multi-Phase Flow and Transport Equations

264   Most applications of the code have reflected ParFlow's core functionality as a single-phase

265   flow solver, but there are also embedded capabilities for multi-phase flow of immiscible fluids and

266   solute transport. Multi–phase systems are distinguished from single–phase systems by the presence

267   of one or more interfaces separating the phases, with moving boundaries between phases. The flow

268   equations that are solved in multi–phase systems in a porous medium comprise a set of mass

269   balance and momentum equations. The equations are given by:

270    $$\frac{\partial}{\partial t}(\phi \rho_i S_i) + \nabla.(\phi \rho_i S_i \vec{v}_i) - \rho_i Q_i = 0, \qquad (14)$$

271    $$\phi S_i \vec{v}_i + \lambda_i.(\nabla p_i - \rho_i \vec{g}) = 0, \qquad (15)$$

272   where $i = 1, \dots, n$ denotes a given phase (such as air or water). In these equations, ϕ is the porosity

273   of the medium $[-]$ which explains the fluid capacity of the porous medium, and for each phase, i,

274    $S_i(\vec{x}, t)$ is the relative saturation $[-]$ which indicates the content of phase i in the porous medium,

275    $\vec{v}_i(\vec{x}, t)$ represent Darcy velocity vector $[LT^{-1}]$, $Q_i(\vec{x}, t)$ stands for source/sink term $[T^{-1}]$, $p_i(\vec{x}, t)$

276   is the average pressure $[ML^{-1}T^{-2}]$, $\rho_i(\vec{x}, t)$ is the mass density $[ML^{-3}]$, λ_i is the mobility

277    $[L^3 TM^{-1}]$, $\vec{g}$ is the gravity vector $[LT^{-2}]$, $\vec{x}$ and t represent space vector and time respectively.

278   ParFlow solves for the pressures on a discrete mesh and uses a time-stepping algorithm based on

279   a mass conservative backward Euler scheme and spatial discretization (a finite volume method).

280   ParFlow's multi–phase flow capability has not been applied in major studies, however, this

281   capability is also available for testing (Ashby et al., 1993; Tompson et al., 1994; Falgout et al.,

282   1999; Maxwell et al., 2016).

283   The transport equations included in the ParFlow package describe mass conservation in a

284   convective flow (no diffusion) with degradation effects and adsorption included along with

285   extraction and injection wells (Beisman et al., 2015; Maxwell et al., 2016). The transport equation

286   is defined as follows:

287 $\left(\frac{\partial}{\partial t}(\phi c_{i,j}) + \lambda_j \phi c_{i,j}\right) + \nabla.\left(c_{i,j}\vec{v}\right) = -\left(\frac{\partial}{\partial t}\left((1-\phi)\rho_s F_{i,j}\right) + \lambda_i (1-\phi)\rho_s F_{i,j}\right) +$

288 $\sum_k^{nI} \gamma_k^{I;i} \chi\Omega_k^I\left(c_{i,j} - c_{i,j}^{-k}\right) - \sum_k^{nE} \gamma_k^{E;i} \chi\Omega_k^E c_{i,j}$ (16)

289 where $c_{i,j}(\vec{x}, t)$ represents concentration fraction of contaminant $[-]$, , λ_i is degradation rate $[\text{T}^{-1}]$,

290 $F_i(\vec{x}, t)$ is the mass concentration $[\text{L}^3\text{M}^{-1}]$, $\rho_s(\vec{x})$ is the density of the solid mass $[ML^{-3}]$, n_I is

291 injection wells $[-]$, $\gamma_k^{I;i}(t)$ is injection rate $[\text{T}^{-1}]$, $\Omega_k^I(\vec{x})$ represent the area of the injection well

292 $[-]$, $c_{i,j}^{-k}(\vec{x}, t)$ is the injected concentration fraction $[-]$, n_E is the extraction wells $[-]$, $\gamma_k^{E;i}(t)$ is

293 extraction rate $[\text{T}^{-1}]$, $\Omega_k^E(\vec{x})$ is an extraction well area $[-]$, $i = 0, \dots, n_{p-1}\left(n_p \in \{1, 2, 3\}\right)$ is the

294 number of phases, $j = 0, \dots, n_c - 1$ represents the number of contaminants, $c_{i,j}$ is the

295 concentration of contaminant j in phase i, k is hydraulic conductivity $[\text{LT}^{-1}]$, $\chi\Omega_k^I$ is the

296 characteristic function of an injection well region, and $\chi\Omega_k^E$ is the characteristic function of an

297 extraction well region. The mass concentration term, $F_{i,j}$ is taken to be instantaneous in time and

298 a linear function of contaminant concentration:

299 $$F_{i,j} = K_{d;j}c_{i,j}$$ (17)

300 where $K_{d;j}$ is the distribution coefficient of the component $[\text{L}^3\text{M}^{-1}]$. The transport/advection

301 equation or convective flow calculation performed by ParFlow offers a choice of a first-order

302 explicit upwind scheme or a second-order explicit Godunov scheme. The advection calculations

303 are discretized as boundary value problems for each primary dimension over each compute cell.

304 The discretization is a fully-explicit, forward Euler first-order accurate in time approach. The

305 implementation of a second-order explicit Godunov scheme (second-order advection scheme)

306 minimizes numerical dispersion and presents accurate computational process at these time scales

307 than either an implicit or lower-order explicit scheme. Stability issue here is that the simulation

308 timestep is restricted via the courant-Friedrichs-Lewy (CFL) condition, which demands that time

309 steps are chosen small enough to ensure that mass not be transported more than one grid cell in a

310 single timestep in order to maintain stability (Beisman, 2007).

311

312 2.5 Computational Grids

313   An accurate numerical approximation of a set of partial differential equations is strongly

314 dependent on the simulation grid. Integrated hydrologic models can use unstructured or structured

315 meshes for the discretization of the governing equations. The choice of grid type to adopt is

316 problem-specific and often a subjective choice since the same domain can be represented in many

317 ways, but there are some clear tradeoffs. For example, structured grid models, such as ParFlow,

318 may be preferred to unstructured grid models because structured grids provide significant

319 advantages in computational simplicity and speed, and are amenable to efficient parallelization

320 (Durbin, 2002; Kumar et al., 2009; Osei-Kuffuor et al., 2014). ParFlow adopts a regular, structured

321 grid specifically for its parallel performance. There are currently two regular grid formulations

322 included in ParFlow, an orthogonal grid and a terrain-following formulation (TFG); both allow for

323 variable vertical discretization (thickness over an entire layer) over the domain.

324   2.5.1 Orthogonal Grid

325   Orthogonal grids have many advantages, and many approaches are available to transform

326 an irregular grid into an orthogonal grid such as conformal mapping. This mapping defines a

327 transformed set of partial differential equations using an elliptical system with "control functions"

328   determined in such a way that the generated grid would be either orthogonal or nearly orthogonal.

329   However, conformal mapping may not allow flexibility in the control of the grid node distribution,

330   which diminishes its usefulness with complex geometries (Mobley and Stewart, 1980; Haussling

331   and Coleman, 1981; Visbal and Knight, 1982; Ryskin and Leal, 1983; Allievi and Calisal, 1992;

332   Eca, 1996).

333   A Cartesian, regular, orthogonal grid formulation is implemented by default in ParFlow,

334   though some adaptive meshing capabilities are still included in the source code. For example,

335   layers within a simulation domain can be made to have varying thickness. The upper portion of

336   Figure 2 shows the standard way topography or any other non-rectangular domain boundaries are

337   represented in ParFlow. The domain limits, and any other internal boundaries, can be defined using

338   grid-independent triangulated irregular network (TIN) files that define a geometry, or a gridded

339   indicator file can be used to define geometric elements. ParFlow uses octree space partitioning

340   algorithm (a grid-based algorithm or mesh generators filled with structured grids) (Maxwell, 2013)

341   to depict complex structures/land surface representations (e.g. topography, watershed boundaries,

342   and different hydrologic facies) in three-dimensional space (Kollet et al., 2010). These land surface

343   features are mapped onto the orthogonal grid, and looping structures that encompass these irregular

344   shapes are constructed (Ashby et al., 1997). The grid cells above ground surface are inactive

345   (shown in upper region of Figure 2) and are stored in the solution vector but not included in the

346   solution.

347   2.5.2 Terrain Following Grid

348   The inactive portion of a watershed defined with an orthogonal grid can be quite large in

349   complex watersheds with high-relief. In these cases, it is advantageous to use a grid that allows

350   these regions to be omitted. ParFlow's structured grid conforms to the topography via

351   transformation by the terrain following grid formulation. This transform alters the form of Darcy's

352   law to incorporate a topographic slope component. For example, subsurface fluxes are computed

353   separately in both x and y directions making use of the terrain following grid transform as:

354
$$q_x = K \sin(\theta_x) + K \frac{\partial p}{\partial y} \cos(\theta_x), \text{ and}$$

355
$$q_y = K \sin(\theta_y) + K \frac{\partial p}{\partial y} \cos(\theta_y) \qquad\qquad (18)$$

356   where q_x and q_y represent source/sink terms, such as fluxes, that include potential recharge flux

357   at the ground surface $[LT^{-1}]$, p is the pressure head $[L]$; K is the saturated hydraulic conductivity

358   tensor , $[LT^{-1}]$, θ is the local angle $[-]$ of topographic slope, S_x and S_y in the x and y directions

359   and may be presented as $\theta_x = \tan^{-1} S_x$ and $\theta_y = \tan^{-1} S_y$ respectively (Weill et al., 2009). The

360   terrain following grid formulation comes handy when solving coupled surface and subsurface

361   flows (Maxwell, 2013). The terrain following grid formulation uses the same surface slopes

362   specified for overland flow to transform the grid, whereas the slopes specified in the orthogonal

363   grid are only used for 2-D overland flow routing and do not impact the subsurface formulation

364   (see Figure 2). Note that TIN files can still be used to deactivate portions of the transformed

365   domain.

366

367   Figure 2 Caption: Representation of orthogonal (upper) and the terrain following (lower) grid

368   formulations and schematics of the related finite difference dependences (left). The i, j, and k are

369   the x, y, and z cell indices

370

371   3. Equation Discretization and Solvers

372   The core of the ParFlow code is its library of numerical solvers. As noted above, in most

373   cases, the temporal discretization of the governing equations uses an implicit (backward Euler)

374   scheme; with cell-centered finite differences in spatial dimensions. Different components of this

375   solution framework have been developed for the various operational modes of ParFlow including

376   an inexact Newton-Krylov nonlinear solver (section 3.1), a multigrid algorithm (section 3.2), and

377   a multigrid-preconditioned conjugate gradient (MGCG) solver in (section 3.3). The conditions,

378   requirements, and constraints on the solvers depend on the specifics of the problem being solved,

379   and some solvers tend to be more efficient (faster overall convergence) than others for a given

380   problem. The core structure of these solvers and some of their implementation details are given

381   below, with an emphasis on the main concepts behind each solver.

382

383   3.1 Newton–Krylov solver for Variably Saturated Flow

384   The cell-centered fully-implicit discretization scheme applied to Richards' equation leads

385   to a set of coupled discrete nonlinear equations that need to be solved at each time step, and, for

386   variably saturated subsurface flow, ParFlow does this with the inexact Newton-Krylov method

387   implemented in the KINSOL package (Hindmarsh et al., 2005; Collier et al., 2015). Newton-

388   Krylov methods were initially utilized in the context of partial differential equations by (Brown

389   and Saad, 1990). In the approach, coupled nonlinear system as a result of discretization of the

390   partial differential equation is solved iteratively. Within each iteration, the nonlinear system is

391   linearized via a Taylor expansion. After linearization, an iterative Krylov method is used to solve

392   the resulting linear Jacobian system (Woodward, 1998; Osei-Kuffuor et al., 2014). For variably

393   saturated subsurface flow, ParFlow uses the GMRES Krylov method (Saad and Schultz, 1986).

394   Figure 3 is a flow chart of the solution technique ParFlow uses to provide approximate solutions

395   to systems of nonlinear equations.

396

397   Figure 3 caption: Working flow chart of ParFlow's solver for linear and non-linear system solution

398

399   The benefit of this Newton-Krylov method is that the Krylov linear solver requires only

400   matrix-vector products. Because the system matrix is the Jacobian of the nonlinear function, these

401   matrix-vector products may be approximated by taking directional derivatives of the nonlinear

402   function in the direction of the vector to be multiplied. This approximation is the main advantage

403   of the Newton-Krylov approach as it removes the requirement for matrix entries in the linear

404   solver. An inexact Newton method is derived from a Newton method by using an approximate

405   linear solver at each nonlinear iteration, as is done in the Newton-Krylov method (Dembo et al.,

406   1982; Dennis and Schabel, 1996). This approach takes advantage of the fact that when the

407   nonlinear system is far from converged, the linear model used to update the solution is a poor

408   approximation. Thus, the convergence criteria of early linear system solve is relaxed. The tolerance

409   required for solution of the linear system is decreased as the nonlinear function residuals approach

410   zero. The convergence rate of the resulting nonlinear solver can be linear or quadratic, depending

411   on the algorithm used. Through the KINSOL package, ParFlow can either use a constant tolerance

412   factor or ones from (Eisenstat and Walker, 1996). Krylov methods can be very robust, but they

413   can be slow to converge. As a result, it is often necessary to implement a preconditioner, or

414   accelerator, for these solvers.

415

416   3.2 Multigrid Solver

417   Multigrid (MG) methods constitute a class of techniques or algorithms for solving

418   differential equations (system of equations) using a hierarchy of discretization (Volker, 1987;

419   Briggs et al., 2000). Multigrid algorithms are applied primarily to solve linear and nonlinear

420   boundary value problems and can be used as either preconditioners or solvers. The most efficient

421   method for preconditioning the linear systems in ParFlow is the ParFlow Multigrid algorithm

422   (PFMG) (Ashby and Falgout, 1996; Jones and Woodward, 2001). Multigrid algorithms arise from

423   discretization of elliptic partial differential equations (Briggs et al., 2000), and, in ideal cases, have

424   convergence rates that do not depend on the problem size. In these cases, the number of iterations

425   remains constant even as problems sizes grow large. Thus, the algorithm is algorithmically

426   scalable. However, it may take longer to evaluate each iteration as problem sizes increase. As a

427   result, ParFlow utilizes the highly efficient implementation of PFMG in the hypre library (Falgout

428   and Yang, 2002).

429   For variably saturated subsurface flow, ParFlow uses the Newton-Krylov method coupled

430   with a multigrid preconditioner to accurately solve for the water pressure (hydraulic head) in the

431   subsurface and diagnoses the saturation field (which is used in determining the water table).

432   (Woodward, 1998; Jones and Woodward, 2000, 2001; Kollet et al., 2010). The water table is

433   calculated for computational cells having hydraulic heads above the bottom of the cells. Generally,

434   a cell is saturated if the hydraulic head in the cell is above the node elevation (cell center) or the

435   cell is unsaturated if the hydraulic head in the cell is below the node elevation. For saturated flow,

436   ParFlow uses the conjugate gradient method also coupled with a multigrid method. It is important

437   to note that subsurface flow systems are usually much larger radially than they are thick, so it is

438   common for the computational grids to have highly anisotropic cell aspect ratios to balance the

439   lateral and vertical discretization. Combined with anisotropy in the permeability field, these high

440   aspect ratios produce numerical anisotropy in the problem, which can cause the multigrid

441   algorithms to converge slowly (Jones and Woodward, 2001). To correct this problem, a

442   semicoarsening strategy or algorithm is employed, where the grid is coarsened in one direction at

443   a time. The direction chosen is the one with the smallest grid spacing i.e. the tightest coupling. In

444   an instance where more than one direction has the same minimum spacing, then the algorithm

445   chooses the direction in the order of x, followed by y, and then in z. To decide on how and when

446   to terminate the coarsening algorithm, Ashby and Falgout (1996)   determined that a

447   semicoarsening down to a $(1 \times 1 \times 1)$ grid is ideal for groundwater problems.

448

449   3.3 Multigrid-Preconditioned Conjugate Gradient (MGCG)

450    ParFlow uses the multigrid-preconditioned conjugate gradient (CG) solver to solve the

451  groundwater equations under steady-state, and fully saturated flow conditions (Ashby and Falgout,

452  1996). These problems are symmetric and positive definite, two properties for which the CG

453  method was designed to target. While CG lends itself to efficient implementations, the number of

454  iterations required to solve a system such as results from discretization of the saturated flow

455  equation increases as the problem size grows. The PFMG multigrid algorithm is used as a

456  preconditioner to combat this growth and results in an algorithm for which the number of iterations

457  required to solve the system grows only minimally. See Ashby and Falgout (1996) for a detailed

458  description of these solvers and the parallel implementation of the multigrid preconditioned CG

459  method in ParFlow (Gasper et al., 2014; Osei-Kuffuor et al., 2014).

460

461    3.4 Preconditioned Newton-Krylov for Coupled Subsurface – Surface Flows

462     As discussed above, coupling between subsurface and surface or overland flow in

463  ParFlow is activated by specifying an overland boundary condition at the top surface of the

464  computational domain, but this mode of coupling allows for activation and deactivation of the

465  overland boundary condition during simulations where ponding or drying occur. Thus, surface-

466  subsurface coupling can occur anywhere in the domain during a simulation and it can change

467  dynamically during the simulation. Overland flow may occur by the Dunne or Horton mechanism

468  depending on local dynamics. Overland flow routing is enabled when the subsurface cells are fully

469  saturated. In ParFlow the coupling between the subsurface and surface flows is handled implicitly.

470  ParFlow solves this implicit system with the inexact Newton-Krylov method described above.

471   However, in this case, the preconditioning matrix is adjusted to include terms from the surface

472   coupling. In the standard saturated or variably saturated case, the multigrid method is given the

473   linear system matrix, or a symmetric version, resulting from discretization of the subsurface model.

474   Because ParFlow uses a structured mesh, these matrices have a defined structure making their

475   evaluation and application of multigrid straightforward. Due to varying topographic height of the

476   surface boundary, where the surface coupling is enforced, the surface effects add non-structured

477   entries in the linear system matrices. These entries increase complexity of the matrix entry

478   evaluations and reduce effectiveness of the multigrid preconditioner. In this case, the matrix-

479   vector products are most effectively performed through computation of the linear system entries,

480   rather than the finite difference approximation to the directional derivative. For the

481   preconditioning, surface couplings are only included if they model flow between cells at the same

482   vertical height i.e. in situations where overland flow boundary conditions are imposed or activated.

483   This restriction maintains the structured property of the preconditioning matrix while still

484   including much of the surface coupling in the preconditioner. Both these adjustments led to

485   considerable speedup in coupled simulations (Osei-Kuffuor et al., 2014).

486

487   4. Parallel Performance Efficiency

488   Scaling efficiency metrics offer a quantitative method for evaluating the performance of

489   any parallel model. Good scaling generally means that the efficiency of the code is maintained as

490   the solution of the system of equations is distributed onto more processors or as the problem

491   resolution is refined and processing resources are added. Scalability can depend on the problem

492   size, the processor number, the computing environment, and the inherent capabilities of the

493   computational platform used e.g. choice of a solver. The performance of ParFlow (or any parallel

494   code) is typically determined through weak and strong scaling (Gustafson, 1988). Weak scaling

495   involves the measurement of code's efficiency in solving problems of increasing size (i.e.

496   describes how the solution time change with change in the number of processors for a fixed

497   problem size per processor). In weak scaling, the simulation time should remain constant, as the

498   size of the problem and number of processing elements grow such that the same amount of work

499   is conducted on each processing element. Following Gustafson (1988), scaled parallel efficiency

500   is given by:

501    $$E(n,p) = \frac{T(n,1)}{T(pn,p)}$$ (19)

502   where $E(n,p)$ denotes parallel efficiency, T represents the run time as a function of the problem

503   size n, which is spread across several processors p. Parallel code is said to be perfectly efficient if

504    $E(n,p) = 1$, and the efficiency decreases as $E(n,p)$ approaches 0. Generally, parallel efficiency

505   decreases   with   increasing   processor   number   as   communication   overhead   between

506   nodes/processors becomes the limiting factor.

507   Strong scaling describes the measurement of how much the simulation or solution time

508   changes with the number of processors for a given problem of fixed total size (Amdahl, 1967). In

509   strong scaling, a fixed size task is solved on a growing number of processors, and the associated

510   time needed for the model to compute the solution is determined (Woodward, 1998; Jones and

511   Woodward, 2000). If the computational time decreases linearly with the processor number, a

512   perfect parallel efficiency, ($E = 1$) results. The value of E is determined using equation (19).

513   ParFlow has been shown to have excellent parallel performance efficiency, even for large problem

514   sizes and processor counts (see Table 1) (Ashby and Falgout, 1996; Kollet and Maxwell, 2006).

515   In situations where ParFlow works in conjunction with or coupled to other subsurface, land surface

516   or atmospheric models (see Section 5) i.e. increased computational complexity by adding different

517   components or processes, improved computational time may not only depend on ParFlow. The

518   computational cost of such an integrated model is extremely difficult to predict because of the

519   nonlinear nature of the system. The solution time may depend on number of factors including the

520   number of degrees of freedom, the heterogeneity of the parameters, which processes are active

521   (e.g. snow accumulation compared to nonlinear snowmelt processes in land surface model or the

522   switching on or off of the overland flow routing in ParFlow). The only way to know how fast a

523   specific problem will run is to try that problem. Many of the studies presented in Table 1 include

524   computational times for problems with different complexities where ParFlow was used. In a

525   scaling study with ParFlow, Maxwell (2013) examined the relative performance of

526   preconditioning the coupled variably saturated subsurface and surface flow system with the

527   symmetric portion or full matrix for the system. Both options use ParFlow's multigrid

528   preconditioner. Solver performance was demonstrated by combining the analytical Jacobian and

529   the non-symmetric linear preconditioner. The study showed that the non-symmetric linear

530   preconditioner presents faster computational times and efficient scaling . A section of the study

531   results is reproduced in Table 1, in addition to other scaling studies demonstrating ParFlow's

532   parallel efficiency. This tradeoff was also examined in Jones and Woodward (2000).

533   It is worth noting that large and/or complex problem sizes (e.g. simulating a large

534   heterogenous domain size with over 8.1 billion unknowns) will always take time to solve directly,

535   but the approach for setting up a problem depends on the specific problem being modeled. Even

536   for one specific kind of model there may be multiple workflows and how to model such complexity

537   becomes sole responsibility of the modeler. The studies involving ParFlow outlined in Table 1

538   provide a wealth of knowledge regarding domain setup for problems of different complexities.

539   Since these are all specific applications, their information will likely be very useful to modelers

540   trying to build a new domain during the setup and planning phases.

541

542   Table 1: Details for the various parallel scaling studies conducted using ParFlow.

543

544   5. Coupling

545   Different integrated models including atmospheric or weather prediction models (e.g. Weather

546   Research Forecasting Model, Advanced Regional Prediction System, Consortium for Small-Scale

547   Modeling), land surface models (e.g. Common Land Model, Noah Land Surface Model), and a

548   subsurface model (e.g. CruchFlow) have been coupled with ParFlow to simulate a variety of

549   coupled earth system effects (see Figure 4(a)). Coupling between ParFlow and other integrated

550   models was performed to better understand the physical processes that occur at the interfaces

551   between the deeper subsurface and ground surface, and between the ground surface and the

552   atmosphere. None of the individual models can achieve this on their own because ParFlow cannot

account for land surface processes (e.g. evaporation), and atmospheric and land surface models generally do not simulate deeper subsurface flows (Ren and Xue, 2004; Chow et al., 2006; Beisman, 2007; Maxwell et al., 2007; Shi et al., 2014). Model coupling can be achieved either via "offline coupling" where models involved in the coupling process are run sequentially and interactions between them is one–way (i.e. information is only transmitted from one model to the other) or "online" where they interact and feedback mechanisms among components are represented (Meehl et al., 2005; Valcke et al., 2009). Each of the coupled models uses its own solver for the physical system it is solving, then information is passed between the models. As long as each model exhibits good parallel performance, this approach still allows for simulations at very high resolution, with a large number of processes (Beven, 2004; Ferguson and Maxwell, 2010; Shen and Phanikumar, 2010; Shi et al., 2014). This section focuses on the major couplings between ParFlow and other codes. We point out specific functions of the individual models as stand–alone codes that are relevant to the coupling process. In addition, information about the role or contribution of each model at the coupling interface (see Figure 4(b)) that connects with ParFlow are presented (Figure 5 shows the communication network of the coupled models). We discuss couplings between ParFlow and its land surface model (a modified version of the original Common Land Model introduced by Dai et al., (2003)), Consortium for Small-Scale Modeling (COSMO), Weather Research Forecasting Model, Advanced Regional Prediction System, and CruchFlow in sections 5.1, 5.2, 5.3, 5.4, and 5.5 respectively.

Figure 4(a) Caption: A pictorial description of the relevant physical environmental features and model coupling. CLM represents the Community Land Model, a stand-alone Land Surface Model

574 (LSM) via which ParFlow couples' COSMO. The modified version of CLM by Dai et al., (2003)

575 and is not shown in Figure 4(a) because it is a module only for ParFlow, not really a stand-alone

576 LSM any longer.

577

578 Figure 4(b) Caption: Schematic showing information transmission at the coupling interface. PF,

579 LSM, and ATM indicate the portions of the physical system simulated by ParFlow, Land Surface

580 Models, and Atmospheric Models respectively. The downward and upward arrows indicate the

581 directions of information transmission between adjacent models. Note: Coupling between ParFlow

582 and CrunchFlow (not shown) occur within the subsurface.

583   5.1 ParFlow–Common Land Model (PF.CLM)

584   The Common Land Model (CLM) is a land surface model designed to complete land-

585 water-energy balance at the land surface (Dai et al., 2003). CLM parameterizes the moisture,

586 energy and momentum balances at the land surface and includes a variety of customizable land

587 surface characteristics and modules, including land surface type (land cover type, soil texture, and

588 soil color), vegetation and soil properties (e.g. canopy roughness, zero-plane displacement, leaf

589 dimension, rooting depths, specific heat capacity of dry soil, thermal conductivity of dry soil,

590 porosity), optical properties (e.g. albedos of thick canopy), and physiological properties related to

591 the functioning of the photosynthesis-conductance model (e.g. green leaf area, dead leaf, and stem

592 area indices). A combination of numerical schemes is employed to solve the governing equations.

593 CLM uses a time integration scheme which proceeds by a split-hybrid approach, where the solution

594 procedure is split into "energy balance" and "water balance" phases in a very modularized structure

595   (Mikkelson et al., 2013; Steiner et al., 2005, 2009). The CLM described here and as incorporated

596   in ParFlow is a modified version of the original CLM introduced by Dai et al., (2003), though the

597   original version was coupled to ParFlow in previous model applications (e.g. Maxwell and Miller,

598   2005). The current coupled model, PF.CLM consist of ParFlow incorporated with land surface

599   model Jefferson et al., (2015), (2017), and Jefferson and Maxwell, (2015). The modified CLM is

600   composed of a series of land surface modules that are called as a subroutine within ParFlow to

601   compute energy and water fluxes (e.g. evaporation and transpiration) to and out of the soil. For

602   example, the modified CLM computes bare ground surface evaporative flux, E_{gr} as

603    $$E_{gr} = -\beta \rho_a u_* q_* \qquad (20)$$

604   where β (dimensionless) denotes soil resistance factor, ρ_a represents air density $[\text{ML}^{-3}]$, u_*

605   represents friction velocity $[\text{LT}^{-1}]$, and q_* (dimensionless) stands for humidity scaling parameter

606   (Jefferson and Maxwell, 2015). Evapotranspiration for vegetated land surface, E_{veg} is computed

607   as

608    $$E_{veg} = \left[R_{pp,dry} + L_w\right] L_{SAI} \left[\frac{\rho_a}{r_b}\left(q_{sat} - q_{af}\right)\right] \qquad (21)$$

609   where r_b is the air density boundary resistance factor $[\text{LT}^{-1}]$, q_{sat} (dimensionless) is saturated

610   humidity at the land surface, and q_{af} (dimensionless) is the canopy humidity. Combination of q_{sat}

611   and q_{af} forms the potential evapotranspiration. The potential evapotranspiration is divided into

612   transpiration $R_{pp,dry}$ (dimensionless) which depends on the dry fraction of the canopy, and

613   evaporation from foliage covered by water L_w (dimensionless). L_{SAI} (dimensionless) is summation

614   of the leaf and stem area indices which estimates the total surface from which evaporation can

615   occur. A detailed description of the equations CLM of PF.CLM uses can be found in Jefferson et

616   al., (2015), (2017), and Jefferson and Maxwell, (2015).

617   PF.CLM simulates variably saturated subsurface flow, surface or overland flow, and

618   above-ground processes. PF.CLM was developed prior to the current community land model (see

619   section 5.2), and the module structure of the current and early versions are different. PF.CLM has

620   been updated over the years to improve its capabilities. PF.CLM was first done in the early 2000's,

621   as an undiversified, a column proof-of-concept model, where data or message was transmitted

622   between the coupled models via input/output files (Maxwell and Miller, 2005). Later, PF.CLM

623   was presented in a distributed or diversified approach with a parallel input/output file structure

624   where CLM is called as a set sequence of steps within ParFlow (Kollet and Maxwell, 2008a).

625   These modifications, for example, were done to incorporate subsurface pressure values from

626   ParFlow into chosen computations (Jefferson and Maxwell, 2015). These, to some extent

627   differentiate the modified version (PF.CLM) from the original CLM by Dai et al., (2003). Within

628   the coupled PF.CLM, ParFlow solves the governing equations for overland and subsurface flow

629   systems and the CLM modules add the energy balance and mass fluxes from the soil, canopy, and

630   root zone that can occur (i.e. interception, evapotranspiration etc.) (Jefferson and Maxwell, 2015).

631   At the coupling interface where the models overlap and undergo online communication (

632   Figure 4(b)), ParFlow calculates and passes soil moisture as well as pressure heads of the

633   subsurface to CLM, and CLM calculates and transmits transpiration from plants, canopy and

634   ground surface evaporation, snow accumulation and melt, and infiltration from precipitation to

635   ParFlow (Ferguson et al., 2016). In short, CLM does all canopy water balances and snow, but once

636   the water through falls to the ground, or snow melts, ParFlow takes over and estimates the water

637   balances via the nonlinear Richards' equation. The coupled model, PF.CLM, has been shown to

638   more accurately predict root-depth soil moisture compared to the uncoupled model i.e. stand-alone

639   land surface model (CLM) with capability of computing near surface soil moisture. This increased

640   accuracy results from the coupling of soil saturations determined by ParFlow and their impacts on

641   other processes including runoff and infiltration (Kollet, 2009; Shrestha et al., 2014; Gebler et al.,

642   2015; Gilbert and Maxwell, 2016). For example, (Maxwell and Miller, 2005) found that

643   simulations of deeper soil saturation (more than 40cm) vary between PF.CLM and uncoupled

644   models, with PF.CLM simulations closely matching the observed data. Table 2 contains

645   summaries of studies conducted with ParFlow coupled to either the original version of CLM by

646   (Dai et al., 2003) or modified CLM (ParFlow with land surface model).

647   5.1.1. ParFlowE–Common Land Model (ParFlowE[CLM])

648   It is well established that ParFlow in conjunction with CLM does perform well in

649   estimating all canopy water and subsurface water balances (Maxwell and Miller, 2005; Mikkelson

650   et al., 2013; Ferguson et al., 2016). ParFlow, as a component of the coupled model has been

651   modified into a new parallel numerical model, ParFlowE to incorporate the more complete heat

652   equation coupled to variably saturated flow. ParFlowE simulates coupling of terrestrial hydrologic

653   and energy cycles i.e. coupled moisture, heat, and vapor transport in the subsurface. ParFlowE is

654   based on the original version of ParFlow having identical solution schemes and coupling approach

655   with CLM. A coupled three-dimensional subsurface heat transport equation is implemented in

656   ParFlowE using a cell-centered finite difference scheme in space and an implicit backward Euler

657   differencing scheme in time. However, the solution algorithm employed in ParFlow is fully

658   exploited in ParFlowE where the solution vector of the Newton-Krylov method was extended to

659   two dimensions (Kollet et al., 2009). In some integrated and climate models, the convection term

660   of subsurface heat flux and the effect of soil moisture on energy transport is neglected due to

661   simplified parameterizations and computational limitations. However, both convection and

662   conduction terms are considered in ParFlowE (Khorsandi et al., 2014). In ParFlowE, functional

663   relationships (i.e. equations of state) are performed to relate density and viscosity to temperature

664   and pressure, and thermal conductivity to saturation. That is, modeling thermal flows by relating

665   these parameterizations in simulating heat flow is an essential component of ParFlowE. In

666   coupling between ParFlowE and CLM, ParFlowE[CLM], the one-dimensional subsurface heat

667   transport in the CLM is replaced by the three-dimensional heat transport equation including the

668   process of convection of ParFlowE. CLM computes mass and energy balances at ground surface

669   that lead to moisture fluxes and pass these fluxes to the subsurface moisture algorithm of

670   ParFlowE[CLM]. These fluxes are used in computing subsurface moisture and temperature fields

671   which are then passed back to the CLM.

672

673   5.2 ParFlow in the Terrestrial Systems Modeling Platform, TerrSysMP

674   ParFlow is part of the Terrestrial System Modeling Platform TerrSysMP, which comprise

675   the nonhydrostatic fully compressible limited-area atmospheric prediction model, COSMO,

676   designed for both operational numerical weather prediction and various scientific applications on

677   the meso–β (horizontal scales of 20–200km) and meso–γ (horizontal scales of 2–20km) (Duniec

678 and Mazur, 2011; Levis and Jaeger, 2011; Bettems et al., 2015), and the Community Land Model

679 version 3.5 (CLM3.5). Currently, it is used in direct simulations of severe weather events triggered

680 by deep moist convection, including intense mesoscale convective complexes, prefrontal squall–

681 line storms, supercell thunderstorms, and heavy snowfall from wintertime mesocyclones. COSMO

682 solves nonhydrostatic, fully compressible hydro–thermodynamical equations in advection form

683 using the traditional finite difference method (Vogel et al., 2009; Mironov et al., 2010; Baldauf et

684 el., 2011; Wagner et al., 2016).

685   An online coupling between ParFlow and the COSMO model is performed via CLM3.5

686 (Gasper et al., 2014; Shrestha et al., 2014; Keune et al., 2016). Similar to the Common Land Model

687 (by (Dai et al., 2003)), CLM3.5 module accounts for surface moisture, carbon, and energy fluxes

688 between the shallow or near-surface soil (discretized/specified top soil layer), snow, and the

689 atmosphere (Oleson et al., 2008). The model components of a fully coupled system consisting of

690 COSMO, CLM3.5, and ParFlow are assembled by making use of the multiple–executable

691 approach (e.g. with OASIS3-MCT model coupler). The OASIS3-MCT coupler employs

692 communication strategies based on the message passing interface standards, MPI1/MPI2 and the

693 Project for Integrated Earth System Modeling, PRISM, Model Interface Library (PSMILe) for

694 parallel communication of two–dimensional arrays between OASIS3-MCT coupler and the

695 coupling models (Valcke et al., 2012; Valcke, 2013). The OASIS3-MCT specifies the series of

696 coupling, frequency of the couplings, the coupling fields, the spatial grid of the coupling fields,

697 transformation type of the (two–dimensional) coupled fields, and simulation time management and

698 integration.

699   At the coupling interface, the OASIS3-MCT interface interchanges the atmospheric

700   forcing terms and the surface fluxes in serial mode. The lowest level and current time step of the

701   atmospheric state of COSMO is used as the forcing term for CLM3.5. CLM3.5 then computes and

702   returns the surface energy and momentum fluxes, outgoing longwave radiation, and albedo to

703   COSMO (Baldauf et al., 2011). The air temperature, wind speed, specific humidity, convective

704   and grid-scale precipitation, pressure, incoming shortwave (direct and diffuse) and longwave

705   radiation, and measurement height are sent from COSMO to CLM3.5. In CLM3.5, a mosaic/tilling

706   approach may be used to represent the subgrid-scale variability of land surface characteristics,

707   which considers a certain number of patches/tiles within a grid cell. The surface fluxes and surface

708   state variables are first calculated for each tile and then spatially averaged over the whole grid cell

709   (Shrestha et al., 2014) . As with PF.CLM3.5, the one–dimensional soil column moisture predicted

710   by CLM3.5 gets replaced by ParFlow's variably saturated flow solver, so ParFlow is responsible

711   for all calculations relating soil moisture redistribution and groundwater flow. Within the

712   OASIS3-MCT ParFlow sends the calculated pressure and relative saturation for the coupled region

713   soil layers to CLM3.5. The CLM3.5 also transmits depth-differentiated source and sink terms for

714   soil moisture including soil moisture flux e.g. precipitation, and soil evapotranspiration for the

715   coupled region soil layers to ParFlow. Applications of TerrSysMP in fully coupled mode from

716   saturated subsurface across the ground surface into the atmosphere include a study on the impact

717   of groundwater on the European heat wave 2003 and the influence of anthropogenic water use on

718   the robustness of the continental sink for atmospheric moisture content (Keune et al., 2016).

719   5.3 ParFlow–Weather Research Forecasting models (PF.WRF)

720   The Weather Research and Forecast (WRF) is a mesoscale numerical weather prediction

721   system designed to be flexible and efficient in a massively parallel computing architecture. WRF

722   is a widely used model that provides a common framework for idealized dynamical studies, full

723   physics numerical weather prediction, air-quality simulations, and regional climate simulations

724   (Michalakes et al., 1999, 2001; Skamarock et al., 2005). The model contains numerous mesoscale

725   physics options such as microphysics parameterizations (including explicitly resolved water vapor,

726   cloud, and precipitation processes), surface layer physics, shortwave radiation, longwave

727   radiation, land surface, planetary boundary layer, data assimilation, and other physics and

728   dynamics alternatives suitable for both large-eddy and global-scale simulations. Similar to

729   COSMO, the WRF model is a fully compressible, conservative-form, non-hydrostatic atmospheric

730   model which uses time-splitting integration techniques (discussed below) to efficiently integrate

731   the Euler equations (Skamarock and Klemp, 2007).

732   The online ParFlow WRF coupling (PF.WRF) extends the WRF platform down to bedrock

733   by including highly resolved three-dimensional groundwater and variably saturated shallow or

734   deep vadose zone flows, and a fully integrated lateral flow above ground surface (Molders and

735   Ruhaak, 2002; Seuffert et al., 2002; Anyah et al., 2008; Maxwell et al., 2011). The land surface

736   model portion that links ParFlow to WRF is supplied by WRF through its land surface component,

737   the Noah Land Surface Model (Ek et al., 2003); the standalone version of WRF has no explicit

738   model of subsurface flow. Energy and moisture fluxes from the land surface are transmitted

739   between the two models via the Noah LSM which accounts for the coupling interface, and which

740   is conceptually identical to the coupling in PF-COSMO. The three-dimensional variably saturated

741   subsurface and two-dimensional overland flow equations, and the three-dimensional atmospheric

742   equations given by ParFlow and WRF are simultaneously solved by the individual model solvers.

743   Land surface processes, such as evapotranspiration, are determined in the Noah LSM as a function

744   of potential evaporation and vegetation fraction. This effect is calculated with the formulation:

745    $$E(x) = F^{fx}(1 - f_{avg})E_{pot} \qquad (22)$$

746   where $E(x)$ stands for rate of soil evapotranspiration (length per unit time), fx represents empirical

747   coefficient, f_{avg} denotes vegetation fraction, and E_{pot} is potential evaporation, determined that

748   depends on atmospheric conditions from the WRF boundary layer parameterization (Ek et al.,

749   2003). The vegetation fraction is zero over bare soils (i.e. only soil evaporation), so equation 22

750   becomes:

751    $$E(x) = F^{fx}E_{pot} \qquad (23)$$

752   The quantity F is parameterized as follows:

753    $$F = \frac{\phi S_w - \phi S_{res}}{\phi - \phi S_{res}}, \qquad (24)$$

754   where ϕ is the porosity of the medium, S_w and S_{res} are relative saturation and residual saturation

755   respectively, from vanGenuchten relationships (VanGenuchten, 1980; Williams and Maxwell,

756   2011). Basically, F refers to the parameterization of the interrelationship between evaporation and

757   near-ground soil water content and provides one of the connections between Noah LSM and

758   ParFlow, and thus WRF.

759   In the presence of a vegetation layer, plant transpiration (length per unit time) is determined

760   as follows:

761
$$T = G(z)C_{plant}f_{veg}E_{pot}, \qquad (25)$$

762   where $C_{plant}(-)$ represents a constant coefficient between 0 and 1, which depends on vegetation

763   species, and the $G(z)$ function represents soil moisture which provides other connection between

764   the coupled models (i.e. ParFlow, Noah, and WRF). The solution procedure of PF.WRF uses an

765   operator–splitting approach where both model components use the same time step. WRF soil

766   moisture information including runoff, surface ponding effects, unsaturated and saturated flow,

767   which includes an explicitly resolved water table are calculated and sent directly to the Noah LSM

768   within WRF by ParFlow and utilized by the Noah LSM in the next time step. WRF supplies

769   ParFlow with evapotranspiration rates and precipitation via the Noah LSM (Jiang et al., 2009).

770   The interdependence between energy and land balance of the subsurface, ground surface, and

771   lower atmosphere can fully be studied with this coupling approach. The coupled PF.WRF via the

772   Noah-LSM has been used to simulate explicit water storage and precipitation within basins, to

773   simulate surface runoffs and to simulate the land-atmosphere feedbacks and wind patterns as a

774   results of subsurface heterogeneity (Maxwell et al., 2011; Williams and Maxwell, 2011). Studies

775   with coupled model PF.WRF are highlighted in Table 2.

776   5.4 ParFlow–Advanced Regional Prediction System (PF. ARPS).

777   The Advanced Regional Prediction System (ARPS) composed of a parallel mesoscale

778   atmospheric model created to explicitly predict convective storms and weather systems. The ARPS

779   platform aids in effectively investigating the changes and predictability of storm-scale weather in

780   both idealized and more realistic settings. The model deals with the three dimensional, fully

781   compressible, non-hydrostatic, spatially filtered Navier-Stokes equations (Rihani et al., 2015). The

782 governing equations include conservation of momentum, mass, water, heat or thermodynamic,

783 turbulent kinetic energy, and the equation of state of moist air making use of a terrain-following

784 curvilinear coordinate system (Xue et al., 2000). The governing equations presented in a

785 coordinate system with z as the vertical coordinate are given as

786
$$\frac{dv}{dt} = -2\Omega \times v - \frac{1}{\rho}\nabla P + g + F \qquad (26)$$

787
$$\frac{d\rho}{dt} = -\rho\nabla.v \qquad (27)$$

788
$$\frac{dT}{dt} = -\frac{RT}{C_v}\nabla.v + \frac{Q}{C_v} \qquad (28)$$

789
$$P = \rho RT \qquad (29)$$

790 Equations (26) to (29) are momentum, continuity, thermodynamic and equation of state,

791 respectively. The material (total) derivative d/dt is defined as

792
$$\frac{d}{dt} = \frac{\partial}{\partial t} + \nabla.v \qquad (30)$$

793 The variables v, ρ, T, P, g, F, Q in equations (26) to (29) represent velocity $[LT^{-1}]$, density

794 $[ML^{-3}]$, temperature [K], pressure $[ML^{-1}T^{-2}]$, gravity $[LT^{-2}]$, frictional force $[MLT^{-2}]$, and the

795 diabatic heat source $[ML^{-2}T^{-2}]$, respectively (Xu et al., 1991). The ARPS model employs high-

796 order monotonic advection technique for scalar transport and fourth-order advection for other

797 variables e.g. mass density and mass mixing ratio. A split-explicit time advancement scheme is

798 utilized with leapfrog on the large time steps, and an explicit and implicit scheme for the smaller

799 time steps is used to inculcate the acoustic terms in the equations (Rihani et al., 2015).

800   The PF.ARPS forms a fully–coupled model that simulates spatial variations in above

801   ground processes and feedbacks, forced by physical processes in the atmosphere and the below the

802   ground surface. In the online coupling process, ARPS land surface model forms the interface

803   between ParFlow and ARPS to transmit information (i.e. surface moisture fluxes) between the

804   coupled models. ParFlow as a component of the coupled model replaces the subsurface hydrology

805   in the ARPS land surface model. Thus, ARPS is integrated into ParFlow as a subroutine to create

806   a numerical overlay at the coupling interphase (specified layers of soil within the land surface

807   model in ARPS) with the same number of soil layers at the ground surface within ParFlow. The

808   solution approach employed is an operator-splitting that allows ParFlow to match the ARPS

809   internal timesteps. ParFlow calculates the subsurface moisture field at each timestep of a

810   simulation and passes the information to ARPS land surface model, which is used in each

811   subsequent timestep. At the beginning of each time step, the surface fluxes from ARPS that are

812   important to ParFlow include evapotranspiration rate and spatially–variable precipitation

813   (Maxwell et al., 2007). PF. ARPS has been applied to investigate the effects of soil moisture

814   heterogeneity on atmospheric boundary layer processes. PF.ARPS keeps a realistic soil moisture

815   that is topographically-driven distribution and shows spatiotemporal relationship between water

816   depth, land surface and lower atmospheric variables (Maxwell et al., 2007; Rihani et al., 2015). A

817   summary of current studies involving PF. ARPS is included in Table 2.

818

819   5.5 ParFlow–CrunchFlow (ParCrunchFlow)

820   CrunchFlow is a software package developed to simulate multicomponent multi-

821   dimensional reactive flow and transport in porous and/or fluid media (Steefel, 2009). Systems of

822   chemical reactions that can be solved by the code include kinetically controlled homogenous and

823   heterogeneous mineral dissolution reactions, equilibrium–controlled homogeneous reactions,

824   thermodynamically controlled reactions, and biologically–mediated reactions (Steefel and Lasaga,

825   1994; Steefel and Yabusaki, 2000). In CrunchFlow, discretization of the governing coupled partial

826   differential equations which connect subsurface kinetic reactions and multicomponent

827   equilibrium, flow and solute transport is based on finite volume. (Li et al., 2007; Li et al., 2010).

828   Coupling of reactions and transport in CrunchFlow that are available at runtimes are performed

829   using two approaches. These are briefly discussed below.

830   First, a global implicit or one–step method approach is based on a backwards Euler time

831   discretization, with a global solution of the coupled reactive transport equations using Newton's

832   method. This global implicit scheme solves the transport and reaction terms simultaneously (up to

833   two-dimensional) (Kirkner and Reeves, 1988; Steefel, 2009). Second, a time or operator splitting

834   of the reaction and transport terms which is based on an explicit forward Euler method; the

835   sequential non-iterative approach, SNIA (in which the transport and reaction terms are solved)

836   (Steefel and Van Cappellen, 1990; Navarre-Sitchler et al., 2011). The stability criteria associated

837   with the explicit approach is that the simulation timestep is restricted via the courant-Friedrichs-

838   Lewy (CFL) condition, under the circumstance that the transportation of mass does not occur over

839   multiple grid cell, but a single grid cell in a timestep. Thus, a small-time step must be used to

840   ensure this condition holds. This small step size may lead to simulations that will demand much

841 time to solve Beisman, (2007), so more processors are used, in order to decrease the processor

842 workload and decrease solution time of the simulation. Coupling of fully saturated flow to the

843 reactive transport calculations and coupling between a partially saturated flow and transport (flow

844 and diffusion) can be done successively. However, these simulations require calculations of the

845 flow and liquid saturation fields with a different model.

846 ParCrunchFlow is a parallel reactive transport model developed by combining ParFlow

847 with CrunchFlow. ParCrunchFlow was designed to be only applicable for subsurface simulation.

848 The coupled model relies on ParFlow's robustness ability to efficiently represent heterogeneous

849 domains and simulate complex flow to provide a more realistic representation of the interactions

850 between biogeochemical processes and non-uniform flow fields in the subsurface than the

851 uncoupled model. ParFlow provides solution of Richards' equation to ParCrunchFlow, which is

852 not present in the biogeochemical code CrunchFlow. ParCrunchFlow employs operator-splitting

853 method to reactive transport, in which the transport and reaction terms are decoupled and

854 calculated independently. Online coupling between the models is achieved through a sequential

855 non-iterative approach, where the reaction terms in CrunchFlow's operator-splitting solver gets

856 connected to ParFlow's advection terms. ParCrunchFlow takes advanatage of multidimensional

857 advection capability of ParFlow instead of CrunchFlow's advective-dispersive transport

858 capabilities (up to two-dimensional). A steady state governing differential equation for reaction

859 and advection (with no dispersion and diffusion terms) in a single-phase system is given by

860
$$\frac{\partial C_i}{\partial t} + \nabla.(vC_i) - R_i = 0, \quad (i = 1, N_{tot})$$
(31)

861 where C_i is the concentration of species i, v represents velocity of flow, R_i indicates total reaction

862 rate of species i, and N_{tot} represents total species number. In the coupling process, the advection

863 terms are calculated by ParFlow's transport solver through a first-order explicit upwind scheme or

864 a second-order explicit Godunov scheme. Low-order upwind weighting schemes can introduce

865 numerical dispersion, which can impact the simulated reactions, and a comparison of several

866 upwinding schemes can be found in (Benson et al., 2017). CrunchFlow calculates the reaction

867 terms using the Newton-Raphson method. For example, in the coupled–model ParCrunchFlow,

868 ParFlow code assigns all hydrological parameters, undertakes the functions relating to

869 parallelization including domain decomposition and message transmission, and solves for pressure

870 and flow fields. The CrunchFlow module is then used to evaluate all reaction terms and

871 conversions between mobile and immobile concentrations. Sequence of simulations of a floodplain

872 aquifer, comprising biologically mediated reduction of nitrate have been performed with

873 ParCrunchFlow. The simulations demonstrate that ParCrunchFlow realistically represents the

874 changes in chemical concentrations seen in most field scale systems than CrunchFlow alone

875 (summarized in Table 2) (Beisman, 2007; Beisman et al., 2015).

876 Figure 5 Caption: Schematic of the communication structure of the coupled models. Note: CLM

877 represents a stand-alone Community Land Model. The modified version of CLM by Dai et al.,

878 (2003) is not shown here because it is a module only for ParFlow, not really a stand-alone LSM

879 any longer.

880

6. Discussion and Summary

IHMs constitute classes of simulation tools ranging from simple lumped parameter models to comprehensive deterministic, distributed and physically based modeling systems for simulation of multiple hydrological processes (LaBolle et al., 2003; Castronova et al., 2013). They are indispensable in studying the interactions between surface and subsurface systems. IHMs that calculate surface and subsurface flow equations in a single matrix (Maxwell et al., 2015), scaling from the beginning parts to the mouth of continental river basins at high-resolutions are essential (Wood, 2009) in understanding and modeling surface-subsurface systems. IHMs have been used to address surface and subsurface science and applied questions. For example, evaluating the effects of groundwater pumping on streamflow and groundwater resources (Markstrom et al., 2008), evaluating relationship between topography and groundwater (Condon and Maxwell, 2015), coupling water flow and transport (Sudicky et al., 2008; Weill et al., 2011) and assessing the resilience of water resources to human stressors or interventions and the variations in the (Maxwell et al., 2015) over large spatial extents at high resolution. Modeling or simulation at large spatial extents e.g. regional and continental scales and resolution e.g. 1km^2 (Figure 6), and even small spatial scale (Figure 7) comes with the associated computational load even on massively parallel computing architectures. IHMs, such as ParFlow have overcome the computational burden of simulating or resolving questions (e.g. involving approximating variably saturated and overland flow equations) beyond such levels of higher spatial scales and resolutions. This capability may not be associated with more conceptually based models which, for example, may not simulate lateral groundwater flow or resolve surface and subsurface flow by specifying zones of

902   groundwater network of stream before performing a simulation (Maxwell et al., 2015) For cross-

903   comparison of ParFlow with other contemporary IHMs, a more comprehensive model testing and

904   analyses have recently been done and readers can access these resources at Maxwell et al., (2014),

905   Koch et al., (2016) and Kollet et al., (2017).

906   Figure 6 Caption: Map of water table depth (m) over the simulation domain with two insets

907   zooming into the North and South Platte River basin, headwaters to the Mississippi River. Colors

908   represent depth in log scale (from 0.01 to 100 m) (Maxwell et al., 2015).

909   Figure 7 Caption: Map of hydraulic conductivity (K) and stream depth in the East Inlet watershed

910   in Colorado (Engdahl and Maxwell, 2015). This domain covers $30km^2$ using 3.1 million $20m^2$

911   (lateral grid cells. The springs emanating from within the hillslopes highlight the realism afforded

912   by integrated modeling at small scales.

913

914   ParFlow is based on efficient parallelism (high performance efficiency) and robust

915   hydrologic capabilities. The model solvers and numerical methods used are powerful, fast, robust,

916   and stable, which has contributed to the code's excellent parallel efficiency. As stated earlier,

917   ParFlow is very capable of simulating flows under saturated and variably saturated conditions i.e.

918   surface, vadose, and groundwater flows, even in highly heterogeneous environments. For example,

919   in simulation of surface flows (i.e. solving the kinematic wave overland flow equations), ParFlow

920   possess the ability to accurately solve streamflow (channelized flow) by using parameterized river

921   routing subroutines (Maxwell and Miller, 2005; Maxwell et al., 2007, 2011). ParFlow includes

coupling capabilities with a flexible coupling interface which has been utilized extensively in resolving many hydrologic problems. The interface-based and process-level coupling used by ParFlow is an example for enabling high-resolution, realistic modeling. However, based on the applications, it would be worthwhile to create one, or several, generic coupling interfaces within ParFlow to make it easier to use its surface/subsurface capabilities in other simulations. Nonetheless, ParFlow has been used in coupling studies in simulating different processes and/or systems including simulating energy and water budgets of the surface and subsurface (Rihani et al., 2010; Mikkelson et al., 2013), surface water and groundwater flows and transport (Kollet and Maxwell, 2006; Beisman, 2007; Beisman et al., 2015; Maxwell et al., 2015), and subsurface, surface, and atmospheric mass and energy balance (Maxwell and Miller, 2005; Maxwell et al., 2011; Shrestha et al., 2014; Sulis et al., 2017). Undoubtedly, such coupled-model simulations come with computational burden and ParFlow performs well in overcoming such problems, even at high spatial scale and resolutions. This capability of ParFlow (coupling with other models) is continuously being exploited by hydrologic modelers, and new couplings are consistently being established. For example, via model coupling, the entire transpiration process could be investigated i.e. from carbon dioxide sequestration from the atmosphere by plants, subsurface moisture dynamics and impacts, to oxygen production by plants. Likewise, land cover change effects on mountain pine beetles may be investigated via coupling of integrated models. But these projected research advances can only be achieved if the scientific community keeps advancing code performance by developing, revising, updating, and rigorously testing these models' capabilities.

942 Presently, ParFlow's open source model and open developer community is fully

943 transparent, and this openness is a major difference between it and other models that has enabled

944 ParFlow to continue evolving. The user community is growing daily across the globe. Code

945 developers have made available, aside from the ParFlow working manual, an active and

946 frequently-updated blog (current blog: "http://parflow.blogspot.com/") and other sources

947 including "https://www.parflow.org" and "https://github.com/parflow" where code developers and

948 experienced users provide great information and suggestions that help in fixing bugs and ease

949 frustrations of other users. Over the years, these easily accessible resources have proven to be

950 helpful. The code is constantly updated through release of new versions with modifications

951 designed to meet varying hydrologic challenges and directions for applications across different

952 scales and fields. Each ParFlow package (version) comes with verified simulation test cases with

953 directions that simulate different real systems and idealized cases. These serve as great resource

954 where additional code modifications have been tested in every release of the code. ParFlow has a

955 clear, rigorous verification procedure to make sure that any changes checked in do not "break"

956 previous developments. This ensures numerical accuracy and backwards compatibility. Moreover,

957 the full suite of test cases is automatically re-run before any submitted change can even be

958 considered for merging with the master branch of the code. The number of branches/forks cannot

959 be controlled in any open source (or community) code, but any contributions to the master branch

960 are exhaustively vetted before being pushed out to users. Further, there is a software development

961 and sustainability plan to improve the capabilities of ParFlow such as incorporation of new

962 formulations of both kinematic and diffusive wave approximations, and advanced parallelization

963   support (GPU's and heterogeneous compute architectures). ParFlow works very well on different

964   computing architectures and operating systems from "Laptops to Supercomputers" (single CPU,

965   Linux clusters, highly scalable systems including IBM Blue Gene) with the same source code and

966   input on all platforms. The code can use significant computational power and runs efficiently on

967   supercomputing environments (e.g. Edison, Cori, JUQUEEN, and Yellowstone). Through

968   ParFlow hydrologic modelers have available a very efficient yet still growing integrated

969   hydrologic model to simulate and understand surface-subsurface flows.

970   Code availability

971   ParFlow is an open–source, object–oriented, parallel watershed flow model developed by
972   community of scientists from the Environmental Protection Department at the Lawrence
973   Livermore National Laboratory (LLNL), Colorado School of Mines and F-Z Jülich with
974   supporting scientists from several other institutions. The current version of ParFlow is available
975   at: https://github.com/parflow/parflow/releases/tag/v3.6.0. The version of ParFlow described in
976   this manuscript is archived on zenodo: https://doi.org/10.5281/zenodo.3555297.

977   Author Contribution

978   Section 3 of the manuscript was written by Carol S. Woodward. Benjamin N. O. Kuffour and
979   Nicholas B. Engdahl wrote the other Sections, and the entire manuscript was edited by Laura E.
980   Condon, Stefan Kollet, and Reed M. Maxwell.

981   Competing Interest

982   We declare that no conflict of interest exist whatsoever between any of the authors and the editors
983   or the referees.

984   Acknowledgement

985   We kindly acknowledge funding of the project by the U.S. Department of Energy, Office of
986   Science (Subsurface Biogeochemical Research), Award number DE-SC0019123.

987

988

989

990

991

992

993

994

995

996

997

998   FIGURES

999
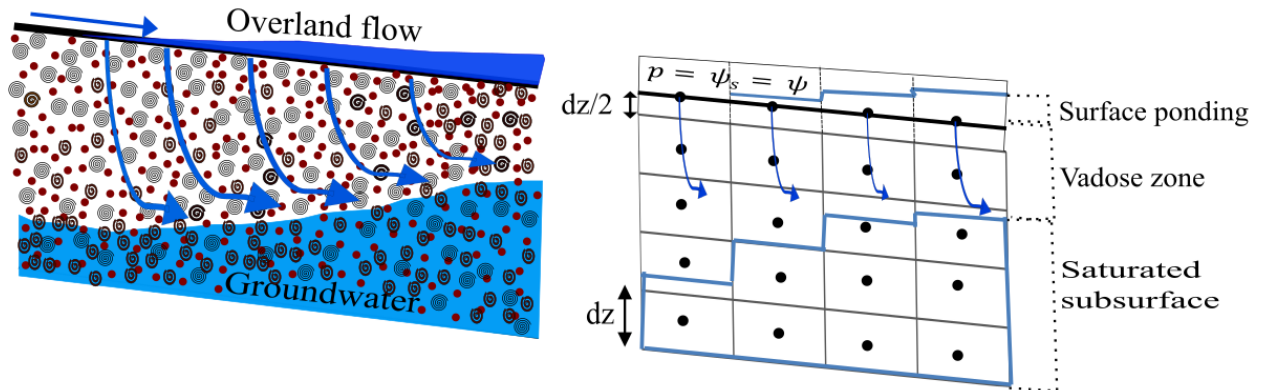
Figure 1: Coupled surface and subsurface flow systems. The physical system is represented on the

left and a schematic of the overland flow boundary condition (continuity of pressure and flux at

the ground surface) is on the right. The equation, $p = \psi_s = \psi$ in Figure 1 signifies that at the

ground surface, the vertically averaged surface pressure and subsurface pressure head are equal,

which is the unique overland flow boundary used by ParFlow.

1005

1006

1007
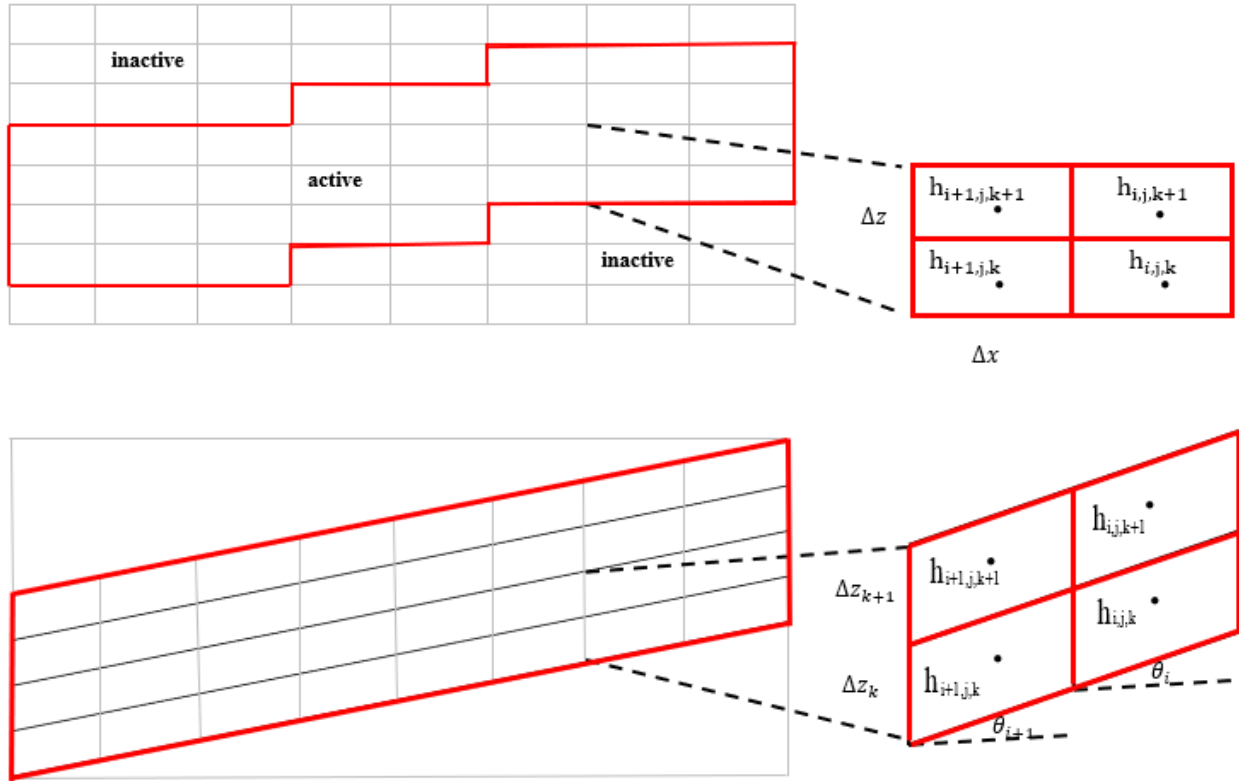
1008   Figure 2: Representation of orthogonal (upper) and the terrain following (lower) grid formulations

1009   and schematics of the associated finite difference dependences (right). The i, j, and k are the x, y,

1010   and z cell indices

1011

1012

1013

1014

1015

1016

1017

1018

1019

1020

1021

1022

1023

1024

1025

1026

1027

1028

1029

1030

1031

1032

1033

1034

1035

1036

1037

1038
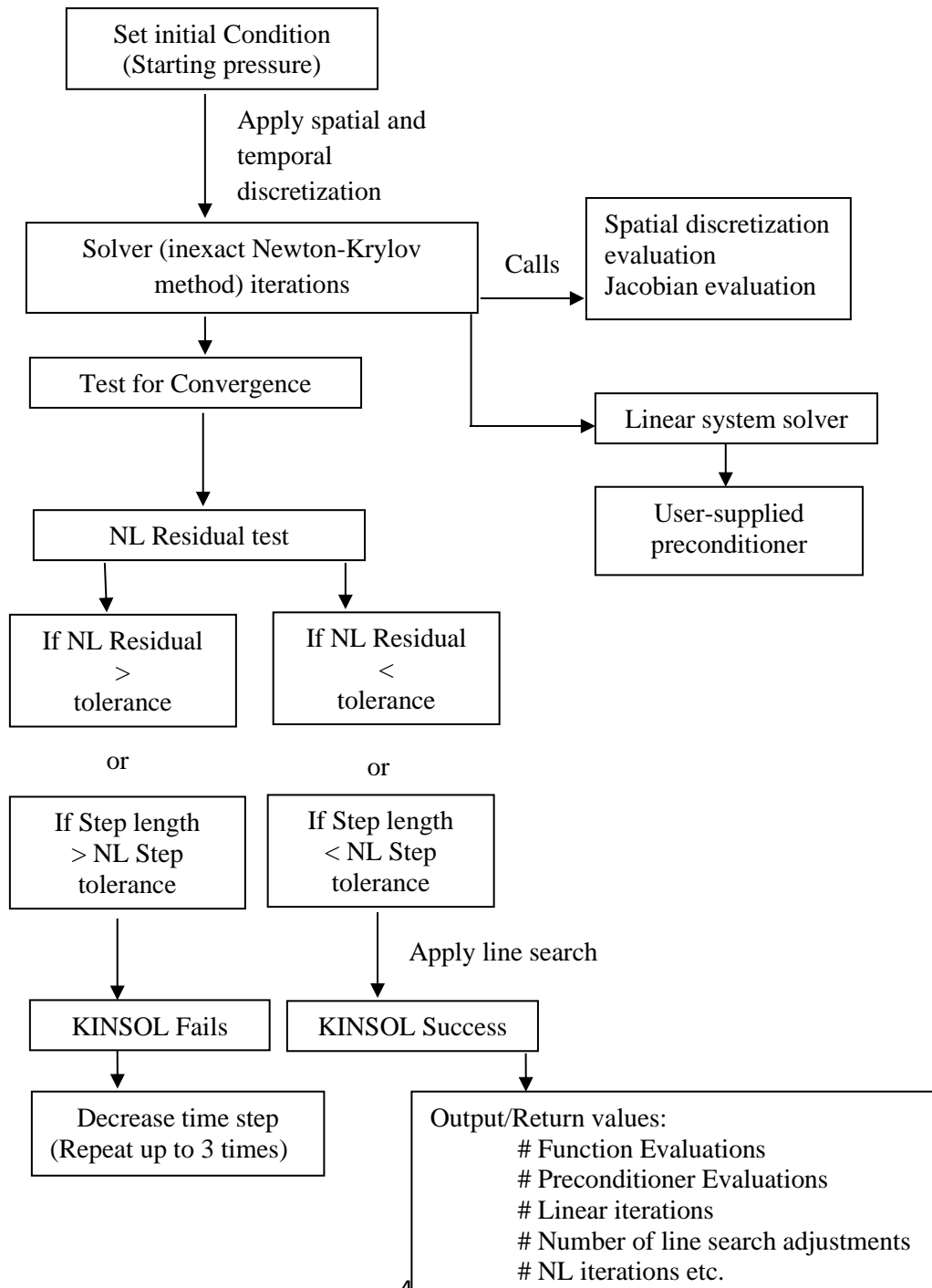
1039   Figure 3: Working flow chart of ParFlow's solver for linear and non-linear system solution

1040
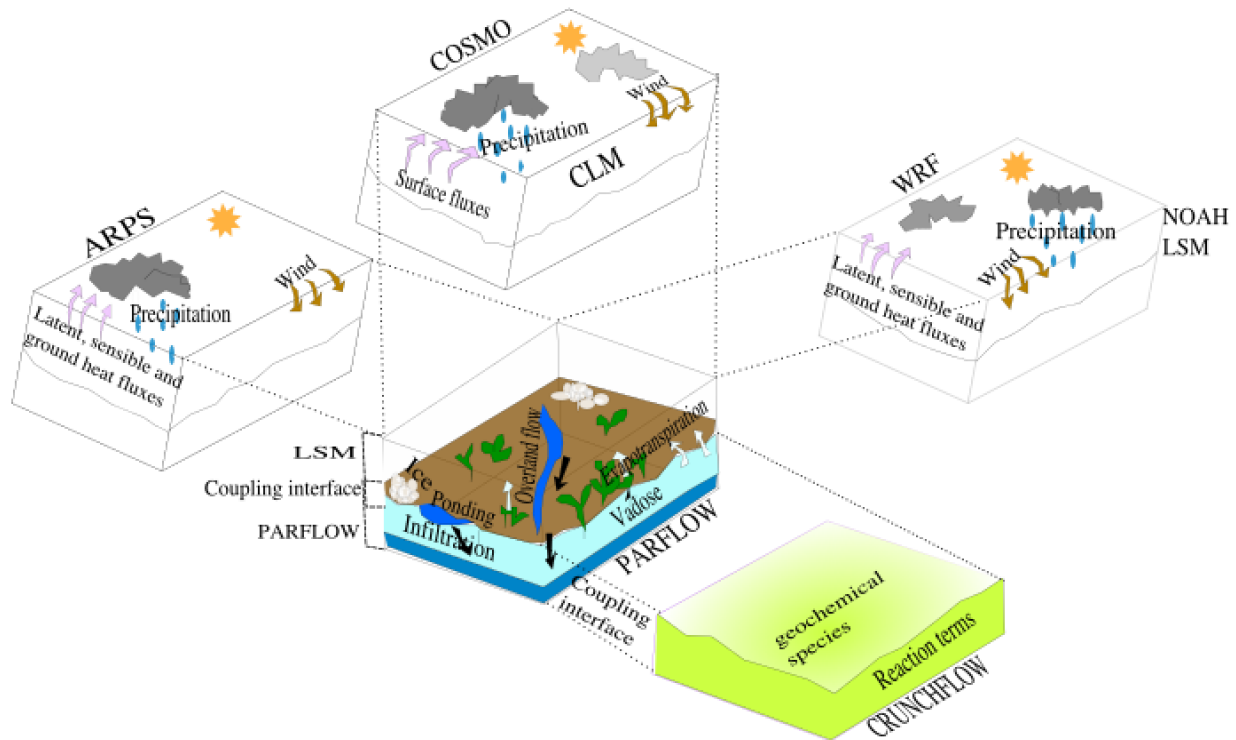
1041
1042   Figure 4(a): A pictorial description of the relevant physical environmental features and model

1043   coupling. CLM represents the Community Land Model, a stand-alone Land Surface Model (LSM)

1044   via which ParFlow couples' COSMO. The modified version of CLM by Dai et al., (2003) and is

1045   not shown in Figure 4(a) because it is a module only for ParFlow, not really a stand-alone LSM

1046   any longer. The core model (ParFlow) always solves the variably saturated 3-D groundwater flow

1047   problem but the various couplings add additional capabilities.

1048

1049
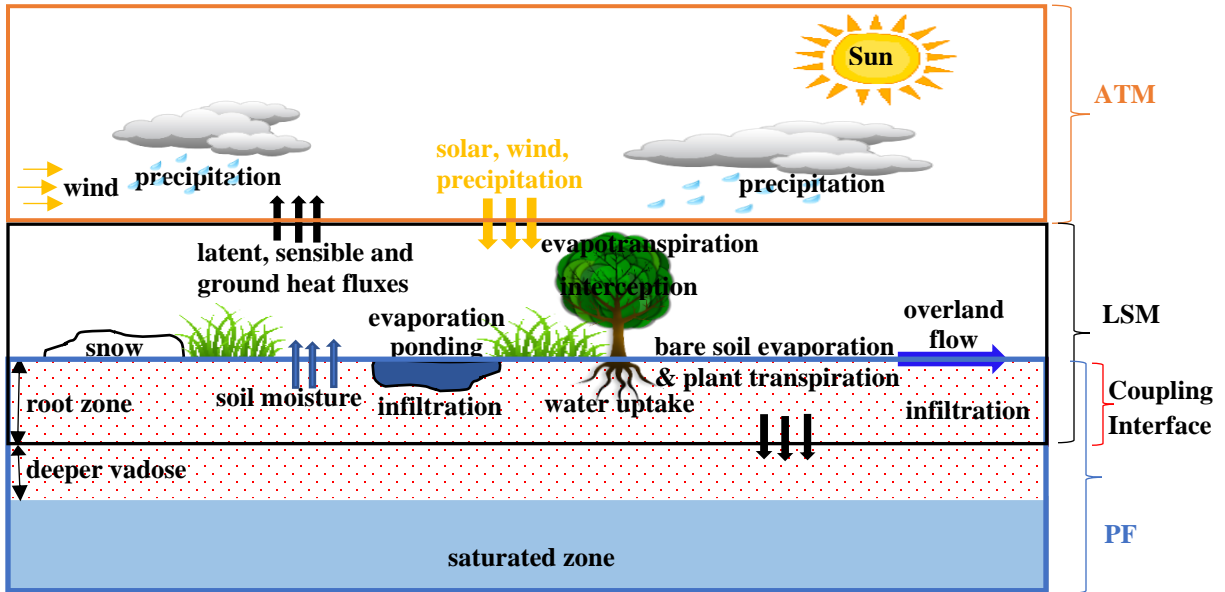
Figure 4(b): Schematic showing information transmission at the coupling interface. PF, LSM, and ATM indicate the portions of the physical system simulated by ParFlow, Land Surface Models, and Atmospheric Models respectively. The downward and upward arrows indicate the directions of information transmission between adjacent models. Note: Coupling between ParFlow and CrunchFlow (not shown) occur within the subsurface.

1073

1074

1075

1076

1077

1078

1079

1080

1081

1082

1083
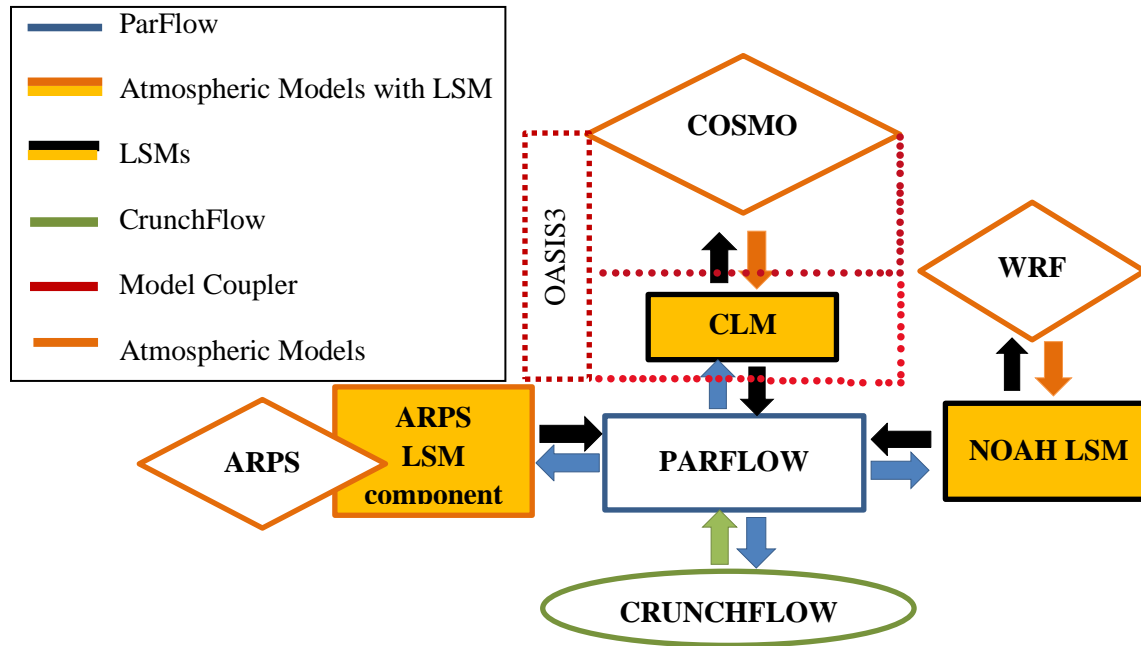
Figure 5: Schematic of the communication structure of the coupled models. Note: CLM represents a stand-alone Community Land Model. The modified version of Common Land Model by Dai et al., (2003) is not shown here because it is a module only for ParFlow, not really a stand-alone LSM any longer.

1084
1085
1086

1087

1088

1089

1090

1091

1092
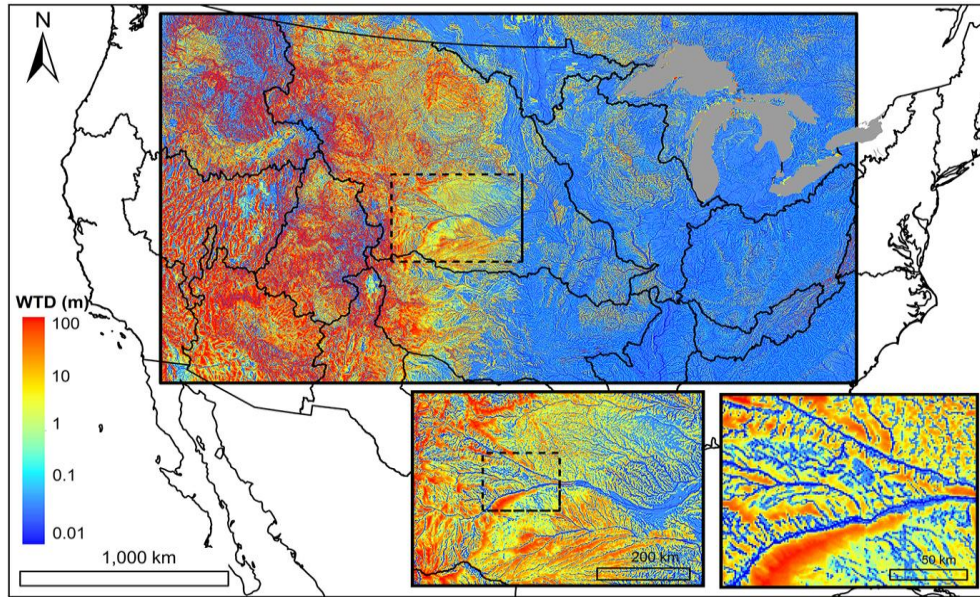
1093 Figure 6: Map of water table depth (m) over the simulation domain with two insets zooming into

1094 the North and South Platte River basin, headwaters to the Mississippi River. Colors represent depth

1095 in log scale (from 0.01 to 100 m) (reproduced from Maxwell et al., 2015). The domain uses 1km^2

1096 grid cells and represents one of the largest, and highest resolution domains simulated by integrated

1097 models to date.

1098
1099

1100

1101

1102
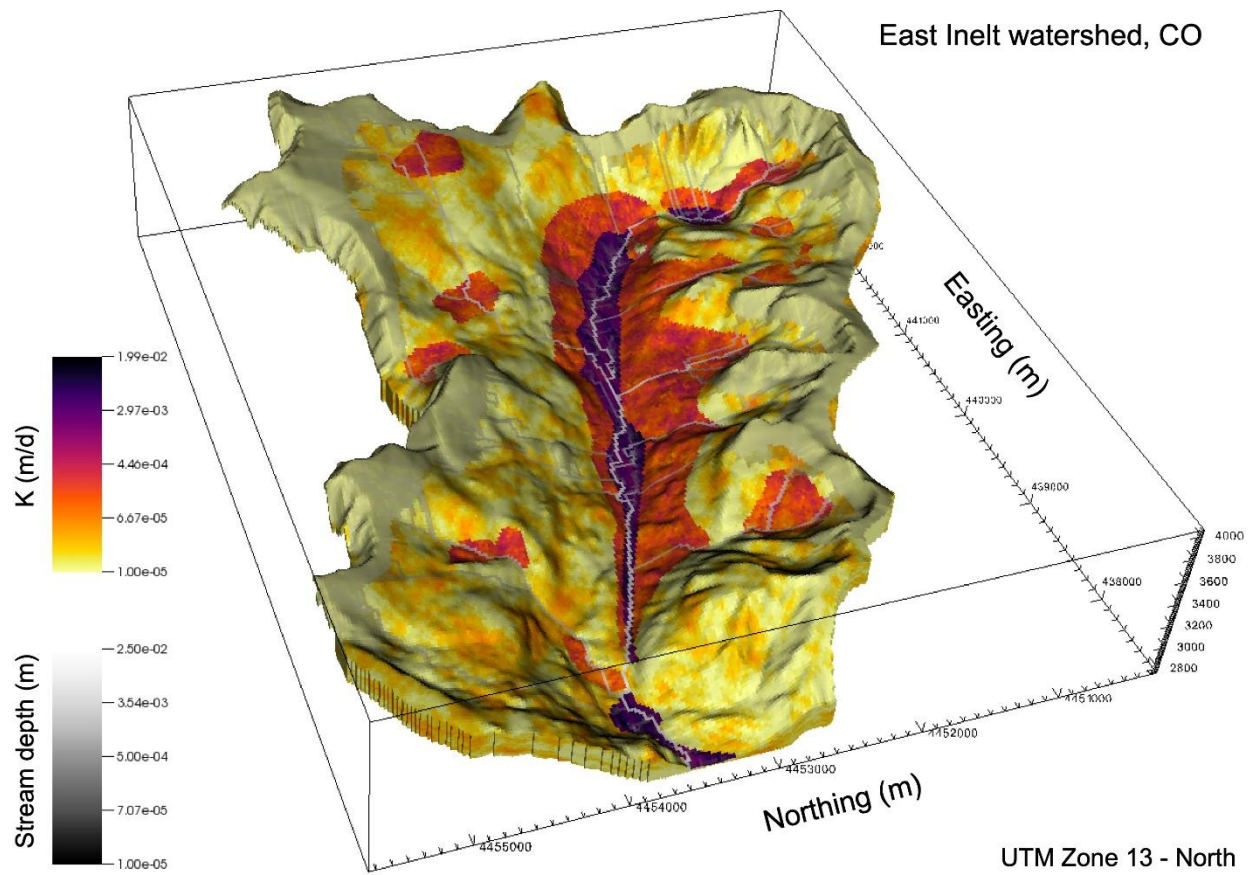
1103 Figure 7: Map of hydraulic conductivity (K) and stream depth in the East Inlet watershed in

1104 Colorado (Engdahl and Maxwell, 2015). This domain covers 30km^2 using 3.1 million lateral grid

1105 cells. The springs emanating from within the hillslopes highlight the realism afforded by integrated

1106 modeling at small scales.

1107

1108

1109

1110   Table 1: Details for the various scaling studies conducted using ParFlow

Simulation Case	Computer System	Processor Number	Jacobian/ Numerical Method	Preconditioner	Computation time (seconds)	Problem Size (cell Number)	Parallel Efficiency (%)	Study
Surface processes and variably saturated flow (ParFlow and CLM)	JUGENE (IBM Blue-Gene Super-computer)	16,384	Finite difference	ParFlow Multigrid	10,920	486,000	58.00	(Kollet et al., 2010)
Terrain Following Grid	JUGENE (IBM Blue-Gene Super-computer)	4,096	Analytical	Non-Symmetric	1,130.50	2,048,000,000	80.91	(Maxwell, 2013)
Overland flow	Intel Xeon Tightly coupled Linux Cluster	100	Finite difference	–	10,800	50,000	82.00	(Kollet and Maxwell, 2006)
Excess infiltration produced runoff	Intel Xeon Tightly coupled Linux Cluster	100	Finite difference	–	10,800	50,000	72.00	(Kollet and Maxwell, 2006)
Terrain Following Grid	JUGENE (IBM Blue-Gene Super-computer)	16,384	Finite difference	Symmetric	2,100.81	8,192,000,000	50.60	(Maxwell, 2013)
Subsurface and Overland flow coupling	IBM BGQ architecture	1,024	Analytical /Finite difference	ParFlow Multigrid	7,200	150,000	50.00	(Osei-Kuffuor et al., 2014)
Fully coupling terrestrial systems modeling platform	IBM BGQ system JUQUEEN	4,096	–	–	–	38,880	82.00	(Gasper et al., 2014)
Performance evaluation of ParFlow code (modified version of ParFlow)	(IBM Blue-Gene Super-computer) JUQUEEN	458,752	Finite difference	–	–	10,569,646,080	–	(Burstedde et al., 2018)

1111   Note: The hyphen "– "shows that information was not provided by the appropriate study

1112

1113 Table 2: Selected coupling studies involving application of ParFlow and atmospheric, land surface, and subsurface models

1114

Application	Coupled Model	Simulation Scale and Size (x, y, and z dimensions)	Model Development	Model Calibration	Study
Surface heterogeneity, surface energy budget	CLM	Watershed (30m x 30m x 84m)			(Reyes et al., 2016)
Sensitivity analysis (evaporation parameterization)	CLM (modified)	Column (1m x 1m x 10m)			(Jefferson and Maxwell, 2015)
Sensitivity of photosynthesis and stomatal resistivity parameters	CLM (modified)	Column (2m x 2m x 10m)			(Jefferson et al., 2017)
Active subspaces; dimension reduction; energy fluxes	CLM (modified)	Hillslope (300m x 300m x 10m)			(Jefferson et al., 2015)
Spin-up behavior; initial conditions watershed	CLM	Regional (75km x 75km x 200m)			(Seck et al., 2015)
Urban processes	CLM	Regional (500m x 500m x 5m)		Yes	(Bhaskar et al., 2015)
Global sensitivity	CLM	Watershed (84km x 75km x 144m)		Yes	(Srivastava et al., 2014)
Entropy production optimization and inference principles	CLM	Hillslope (100m x 100m x 5m)			(Kollet, 2015)
Soil moisture dynamics	CLM	Catchment (1180m x 74m x 1.6m)		Yes	(Zhufeng et al., 2015)
Dual-boundary forcing concept	CLM	Catchment (49km x 49km x 50m)			(Rahman et al., 2015)
Initial conditions; Spin-up	CLM	Catchment; Watershed (28km x 20km x 400m)			(Ajami et al., 2014, 2015)
Groundwater-fed irrigation impacts of natural systems; optimization water allocation algorithm	CLM	Watershed; Sub-watershed (41km x 41km x 100m)			(Condon and Maxwell, 2013, 2014)
Subsurface heterogeneity (land surface fluxes)	CLM	Watershed (209km x 268km x 3502m)			(Condon et al., 2013)
Mountain Pine Beetle	CLM	Hillslope (500m x 1000m x 12.5m)			(Mikkelson et al., 2013)
Groundwater-land surface-atmosphere feedbacks	CLM	Watershed (32km x 45km x 128m)			(Ferguson and Maxwell, 2010, 2011, 2012)
Subsurface heterogeneity (land surface processes)	CLM	Hillslope (250m x 250m x 4.5m)			(Atchley and Maxwell, 2011)

Application	Model	Scale (Domain)			Reference
Computational scaling	CLM	Hillslope (150m x 150m x 240m)			(Kollet et al., 2010)
Subsurface heterogeneity (infiltration in arid environment)	CLM	Hillslope (32km x 45km x 128m)			(Maxwell, 2010)
Subsurface heterogeneity (land energy fluxes)	CLM	Hillslope (5km x 0.1km x 310m)			(Rihani et al., 2010)
Heat and subsurface energy transport (ParFlowE)	CLM	Column (1m x 1m x 10m)	Yes		(Kollet et al., 2009)
Subsurface heterogeneity on evapotranspiration	CLM	Column, Hillslope (32m x 45m x 128m)			(Kollet, 2009)
Subsurface heterogeneity (land-energy fluxes; runoff)	CLM	Watershed; Hillslope (3km x 3km x 30m)			(Kollet and Maxwell, 2008)
Climate change (land-energy feedbacks to groundwater)	CLM	Watershed (3000m x 3000m x 30m)			(Maxwell and Kollet, 2008)
Model development experiment	CLM	Column	Yes		(Maxwell and Miller, 2005)
Subsurface transport	CLM	Aquifer (30m x 15m x 0.6m)			(Tompson et al., 1998, 1999; Maxwell et al., 2003)
Model development (TerrSysMP)	COSMO	Watershed (64km x 64km x 30m)	Yes		(Shrestha et al., 2014)
Implementation and Scaling (TerrSysMP)	COSMO	Continental	Yes		(Gasper et al., 2014)
Groundwater response to ground surface-atmosphere feedbacks	COSMO	Continental (436m x 424m x 103m)	Yes		(Keune et al., 2016)
Atmosphere, DART, data assimilation	WRF	Watershed (15km x 15km x 5m)	Yes		(Williams et al., 2013)
Coupled model development (Atmosphere)	WRF	Watershed (15km x 15km x 5m)	Yes		(Maxwell et al., 2011)
Subsurface heterogeneity (runoff generation)	WRF	Hillslope (3km x 3km x 30m)			(Meyerhoff and Maxwell, 2010)
Subsurface uncertainty to the atmosphere	WRF	Watershed (15km x 15km x 5m)	Yes		(Williams and Maxwell, 2011)
Subsurface transport	ARPS	Watershed (17m x 10.2m x 3.8m)		Yes	(Maxwell et al., 2007)
Terrain and soil moisture heterogeneity on atmosphere	ARPS	Hillslope (5km x 2.5km x 80m)			(Rihani et al., 2015)
Risk Assessment of CO leakage	CRUNCHFLOW	Aquifer (84km x 75km x 144m)		Yes	(Atchley et al., 2013)
Reactive transport heterogeneous saturated subsurface environment	CRUNCHFLOW	Aquifer (120m x 120m x 120m)			(Beisman et al., 2015)

1115   Note: "CLM" show that coupling with ParFlow was by the original Common Land Model or Community Land Model. "CLM (modified)" show that the
1116   modified version of Common Land Model by (Dai et al., 2003) was a module for ParFlow.

References

Abu-El-Sha'r, W. Y., and Rihani, J. F.: Application of the high performance computing techniques of parflow simulator to model groundwater flow at Azraq basin, Water Resour. Manag., 21(2), 409–425, doi:10.1007/s11269-006-9023-5, 2007.

Ajami, H., M. F. McCabe, Evans, J. P., and Stisen, S.: Assessing the impact of model spin-up on surface water-groundwater interactions using an integrated hydrologic model, Water Resour. Res., 50, 1–21, doi:10.1002/2013WR014258.Received, 2014.

Ajami, H., McCabe, M. F., and Evans, J. P.: Impacts of model initialization on an integrated surface water-groundwater model, Hydrol. Process., 29(17), 3790–3801, doi:10.1002/hyp.10478, 2015.

Allievi, A., and Calisal, S. M.: Application of Bubnov-Galerkin formulation to orthogonal grid generation, J. Comput. Phys., 98(1), 163–173, doi:10.1016/0021-9991(92)90181-W, 1992.

Amdahl, G. M.: Validity of the single processor approach to achieving large scale computing capabilities, in spring joint computer conference, vol. 37, 256–9, 1967.

Anyah, R. O., Weaver, C. P., Miguez-Macho, G., Fan, Y., and Robock, A.: Incorporating water table dynamics in climate modeling: 3. Simulated groundwater influence on coupled land-atmosphere variability, J. Geophys. Res. Atmos., 113(7), 1–15, doi:10.1029/2007JD009087, 2008.

Ashby, S. F., and Falgout, R. D.: A Parallel Multigrid Preconditioned Conjugate Gradient Algorithm for Groundwater Flow Simulations, Nucl. Sci. Eng., 124, 145–159, 1996.

Ashby, S. F., Falgout, R. D., Smith, S. G., and Tompson, A. F. B.: Modeling groundwater flow on MPPs, Proc. Scalable Parallel Libr. Conf., 17–25, doi:10.1109/SPLC.1993.365586, 1993.

Ashby, S. F., Falgout, R. D., Tompson, A., and Fogwell, T.: Numerical simulation of groundwater flow on MPPs, , 17–25, 1994.

Ashby, S. F., Falgout, R. D., and Tompson, A. F. B.: A Scalable Approach to Modeling Groundwater Flow on Massively Parallel Computers, in In Next Generation Environmental Models and Computational Methods, vol. 87, 201, 1997.

Atchley, A. L., and Maxwell, R. M.: Influences of subsurface heterogeneity and vegetation cover on soil moisture, surface temperature and evapotranspiration at hillslope scales, Hydrogeol. J., 19(2), 289–305, doi:10.1007/s10040-010-0690-1, 2011.

Atchley, A. L., Maxwell, R. M., and Navarre-Sitchler, A. K.,:Human health risk assessment of CO2 leakage into overlying aquifers using a stochastic, geochemical reactive transport approach, Environ. Sci. Technol., 47(11), 5954–5962, doi:10.1021/es400316c, 2013.

Baldauf, M., Seifert, A., Forstner, J., Majewski, D., and Raschendorfer, M.: Operational Convective-Scale Numerical Weather Prediction with the COSMO Model : Description and Sensitivities, Am. Meteorol. Soc., 3887–3905, doi:10.1175/MWR-D-10-05013.1, 2011.

Beisman, J.: Development of a parallel reactive transport model with spatially variable nitrate reduction in a floodplain aquifer, 2007.

Beisman, J. J., Maxwell, R. M., Steefel, C. I., and Molins, S.: ParCrunchFlow : an efficient , parallel reactive transport simulation tool for physically and chemically heterogeneous saturated subsurface environments, 403–422, doi:10.1007/s10596-015-9475-x, 2015a.

Beisman, J. J., Maxwell, R. M., Navarre-Sitchler, A. K., Steefel, C. I., and Molins, S.: ParCrunchFlow: an efficient, parallel reactive transport simulation tool for physically and chemically heterogeneous saturated subsurface environments, Comput. Geosci., 19(2), 403–

1162   422, doi:10.1007/s10596-015-9475-x, 2015b.

1163 Bell, J. B., Dawson, C. N., and Shubin, G. R.: An unsplit, higher order godunov method for
1164   scalar conservation laws in multiple dimensions, J. Comput. Phys., 74(1), 1–24,
1165   doi:10.1016/0021-9991(88)90065-4, 1988.

1166 Benson, D. A., Aquino, T., Bolster, D. N. E. C, and Christopher, D. F.G., Henri, V.: A
1167   comparison of Eulerian and Lagrangian transport and non-linear reaction algorithms, Adv.
1168   Water Resour., 99, 15–37, 2017.

1169 Bettems, J. M., Asensio, H., Bonafe, Duniec, G., Fuhrer, O., Helmert, J., Heret, C., Kazakova,
1170   E., Lange, Machulskaya, E., Mazur, A., De Morsier, G., Rianna, G., Rozinkina, I., Vieli, B.,
1171   Vogel, G.:The COSMO Priority Project "COLOBOC": Final Technical Report No 27, (No
1172   27), 2015.

1173 Beven, K.: Robert E. Horton's perceptual model of infiltration processes, Hydrol. Process.,
1174   18(17), 3447–3460, doi:10.1002/hyp.5740, 2004.

1175 Bhaskar, A. S., Welty, C., Maxwell, R. M., and Miller, A. J.: Untangling the effects of urban
1176   development on subsurface storage in Baltimore, Water Resour. Res., 51(2), 1158–1181,
1177   doi:10.1002/2014WR016039, 2015.

1178 Bixio, A. C., Gambolati, A. G., Paniconi, A. C., Putti, A. M., Shestopalov, A. V. M., Bublias, V.
1179   N., Bohuslavsky, A. A. S., Kasteltseva, A. N. B., and Rudenko, Y. F.: Modeling
1180   groundwater-surface water interactions including effects of morphogenetic depressions in
1181   the Chernobyl exclusion zone, Environ. Geol., 42(162–177), doi:10.1007/s00254-001-0486-
1182   7, 2002.

1183 Briggs, W. L., Henson, V. E., and McCormick, S. F.: A Multigrid Tutorial, Second Edition,
1184   2000.

1185 Brookfield, A. E., Sudicky, E. A., Park, Y. J., and Conant, B.: Thermal transport modelling in a
1186   fully integrated surface/subsurface framework, Hydrol. Process., 23(15), 2150–2164,
1187   doi:10.1002/hyp.7282, 2009.

1188 Brown, P. N., and Saad, Y.: Hybrid Krylov Methods for Nonlinear Systems of Equations, SIAM
1189   J. Sci. Stat. Comput., 11(3), 450–481, doi:10.1137/0911026, 1990.

1190 Burstedde, C., Fonseca, J. A., and Kollet, S.: Enhancing speed and scalability of the ParFlow
1191   simulation code, Comput. Geosci., 22(1), 347–361, doi:10.1007/s10596-017-9696-2, 2018.

1192 Camporese, M., Paniconi, C., Putti, M., and Orlandini, S.: Surface-subsurface flow modeling
1193   with path-based runoff routing, boundary condition-based coupling, and assimilation of
1194   multisource observation data, Water Resour. Res., 46(2), doi:10.1029/2008WR007536,
1195   2010.

1196 Castronova, A. M., Goodall, J. L., and Ercan, M. B.: Integrated Modeling within a Hydrologic
1197   Information System: An OpenMI Based Approach, Environ. Model. Softw.,
1198   doi:10.1016/j.envsoft, 2013.

1199 Celia, M. A., Bouloutas, E. T., and Zarba, R. L.: A general mass-conservative numerical
1200   solution for the unsaturated flow equation, Water Resour. Res., 26(7), 1483–1496,
1201   doi:10.1029/WR026i007p01483, 1990.

1202 Chow, F. K., Kollet, S. J., Maxwell, R. M., and Duan, Q.: Effects of Soil Moisture Heterogeneity
1203   on Boundary Layer Flow with Coupled Groundwater, Land-Surface, and Mesoscale
1204   Atmospheric Modeling, 17th Symp. Bound. Laters Turbul., doi:10.1016/j.phrs.2010.10.003,
1205   2006.

1206 Collier, A. M., Hindmarsh, A. C., Serban, R., and Woodward, C. S.: User Documentation for
1207   kinsol v2.8.2 (SUNDIALS v2.6.2), , 1, 120, 2015.

1208 Condon, L. E., and Maxwell, R. M.: Implementation of a linear optimization water allocation
1209   algorithm into a fully integrated physical hydrology model, Adv. Water Resour., 60, 135–
1210   147, doi:10.1016/j.advwatres.2013.07.012, 2013.
1211 Condon, L. E., and Maxwell, R. M.: Groundwater-fed irrigation impacts spatially distributed
1212   temporal scaling behavior of the natural system: a spatio-temporal framework for
1213   understanding water management impacts, Environ. Res. Lett., 9(3), 034009,
1214   doi:10.1088/1748-9326/9/3/034009, 2014.
1215 Condon, L. E., and Maxwell, R.M.: Evaluating the relationship between topography and
1216   groundwater using outputs from a continental-scale integrated hydrology model, Water
1217   Resour. Res., 51(8), 6602–6621, doi:10.1002/2014WR016774, 2015.
1218 Condon, L. E., Maxwell, R. M., and Gangopadhyay, S.: The impact of subsurface
1219   conceptualization on land energy fluxes, Adv. Water Resour., 60, 188–203,
1220   doi:10.1016/J.ADVWATRES.2013.08.001, 2013.
1221 Condon, L. E., Hering, A. S., and Maxwell, R. M.: Quantitative assessment of groundwater
1222   controls across major US river basins using a multi-model regression algorithm, Adv. Water
1223   Resour., 82, 106–123, doi:10.1016/J.ADVWATRES.2015.04.008, 2015.
1224 Dai, Y. et al.: The Common Land Model, Bull. Am. Meteorol. Soc., 84(8), 1013–1023,
1225   doi:10.1175/BAMS-84-8-1013, 2003.
1226 Dembo, R. S., and Eisenstat, S. C.: Inexact newton methods, in SIAM J. Numer. Anal., vol. 19,
1227   pp. 400–408, 1982.
1228 Dennis Jr, John E., and R. B. S.: Numerical Methods for Unconstrained Optimization and
1229   Nonlinear Equations, 1996.
1230 Duniec, G., and Mazur, A.: COLOBOC - MOSAIC parameterization in COSMO model v. 4.8,
1231   (11), 69–81, 2011.
1232 Durbin, P.: An Approach to Local Refinement of Structured Grids An Approach to Local
1233   Refinement of Structured Grids, J. Comput. Phys., 181, 639–653,
1234   doi:10.1006/jcph.2002.7147, 2002.
1235 Eca, L.: 2D orthogonal grid generation with boundary point distribution control, J. Comput.
1236   Phys., 125(2), 440–453, doi:10.1006/jcph.1996.0106, 1996.
1237 Eisenstat, S. C., and Walker, H. F.: Choosing the Forcing Terms in an Inexact Newton Method,
1238   SIAM J. Sci. Comput., 17(1), 16–32, doi:10.1137/0917003, 1996.
1239 Ek, M. B., Mitchell, K. E., Lin, Y., Rogers, E., Grunmann, P., Koren, V., Gayno, G., and
1240   Tarpley, J. D.: Implementation of Noah land surface model advances in the National
1241   Centers for Environmental Prediction operational mesoscale Eta model, J. Geophys. Res.
1242   Atmos., 108(D22), doi:10.1029/2002JD003296, 2003.
1243 Engdahl, N. B., and Maxwell, R. M.: Quantifying changes in age distributions and the
1244   hydrologic balance of a high-mountain watershed from climate induced variations in
1245   recharge, J. Hydrol., 522, 152–162, doi:10.1016/j.jhydrol.2014.12.032, 2015.
1246 Engdahl, N. B., McCallum, J. L., and Massoudieh, A.: Transient age distributions in subsurface
1247   hydrologic systems, J. Hydrol., 543, 88–100, doi:10.1016/J. Hydrol.2016.04.066, 2016.
1248 Falgout, R. D., and Yang, U. M.: Hypre: A Library of High Performance Preconditioners, in
1249   International Conference on Computational Science., 632–641, Springer, Berlin, 2002.
1250 Falgout, R. D., Baldwin, C., Bosl, W., Hornung, R., Shumaker, D., Smith, S., Woodward, C. S.,
1251   and Tompson, A. F. B.: Enabling Computational Technologies for Subsurface Simulations,
1252   1999.
1253 Ferguson, I. M., and Maxwell, R. M.: Groundwater-Land Surface-Atmosphere Feedbacks:

Impacts of Groundwater Pumping and Irrigation on Land-Atmosphere Interactions, Proc. xviii Int. Conf. Comput. Methods Water Resour., 722–729, 2010.

Ferguson, I. M., and Maxwell, R. M.: Human impacts on terrestrial hydrology: climate change versus pumping and irrigation, Environ. Res. Lett., 7(4), 044022, doi:10.1088/1748-9326/7/4/044022, 2012.

Frei, S., Fleckenstein, J. H., Kollet, S. J., and Maxwell, R. M.: Patterns and dynamics of river-aquifer exchange with variably-saturated flow using a fully-coupled model, J. Hydrol., 375(3–4), 383–393, doi:10.1016/j.jhydrol.2009.06.038, 2009.

Gasper, F., Goergen, K., Shrestha, P., Sulis, M., Rihani, J., Geimer, M., and Kollet, S. J.: Implementation and scaling of the fully coupled Terrestrial Systems Modeling Platform (TerrSysMP v1.0) in a massively parallel supercomputing environment - A case study on JUQUEEN (IBM Blue Gene/Q), Geosci. Model Dev., 7(5), 2531–2543, doi:10.5194/gmd-7-2531-2014, 2014.

Gebler, S., Kollet, S., Qu, W., and Vereecken, H.: High resolution modelling of soil moisture patterns with ParFlow-CLM : Comparison with sensor network data, , 17, 2015, 2015.

Gilbert, J. M., and Maxwell, R. M.: Examining regional groundwater-surface water dynamics using an integrated hydrologic model of the San Joaquin River basin, Hydrol. Earth Syst. Sci. Discuss., 1–39, doi:10.5194/hess-2016-488, 2016.

Gustafson, J. L.: Reevaluating amdahl's law, 31(5), 532–533, 1988.

Haussling, H. ., and Coleman, R.: A method for generation of orthogonal and nearly orthogonal boundary-fitted coordinate systems, J. Comput. Phys., 43(2), 373–381, doi:10.1016/0021-9991(81)90129-7, 1981.

Hindmarsh, A. C., Brown, P. N., Grant, K. E., Lee, S. L., Serban, R., Shumaker, D. E., and Woodward, C. S.: SUNDIALS: Suite of nonlinear and differential/algebraic equation solvers, ACM Trans. Math. Softw., 31(3), 363–396, doi:10.1145/1089014.1089020, 2005.

Ian F. M., Jefferson, J. L., Maxwell, R. M., Kollet, S. J.: Effects of root water uptake formulation on simulated water and energy budgets at local and basin scales, Env. Earth Sci, 75(316), doi:DOI 10.1007/s12665-015-5041-z, 2016.

Ivanov, V. Y., Vivoni, E. R., Bras, R. L., and Entekhabi, D.: Catchment hydrologic response with a fully distributed triangulated irregular network model, Water Resour. Res., 40(11), 1–23, doi:10.1029/2004WR003218, 2014.

Jefferson, J. L., and Maxwell, R. M.: Evaluation of simple to complex parameterizations of bare ground evaporation, J. Adv. Model. Earth Syst., 7, 1075–1092, doi:10.1002/2014MS000398. Received, 2015.

Jefferson, J. L., Gilbert, J. M., Constantine, P. G., and Maxwell, R.M.: Active subspaces for sensitivity analysis and dimension reduction of an integrated hydrologic model, Comput. Geosci., 83, 127–138, doi:10.1016/j.cageo.2015.07.001, 2015.

Jefferson, J. L., Maxwell,R. M., and Constantine, P. G.: Exploring the Sensitivity of Photosynthesis and Stomatal Resistance Parameters in a Land Surface Model, J. Hydrometeorol., 18(3), 897–915, doi:10.1175/JHM-D-16-0053.1, 2017.

Jiang, X., Niu, G. Y., and Yang, Z. L.: Impacts of vegetation and groundwater dynamics on warm season precipitation over the Central United States, J. Geophys. Res. Atmos., 114(6), 1–15, doi:10.1029/2008JD010756, 2009.

Jones, J. E., and Woodward, C. S.: Preconditioning Newton- Krylov Methods for Variably Saturated Flow, in 13th International Conference on Computational Methods in Water Resources, Calgary, Alberta, Canada, 2000.

Jones, J. E., and Woodward, C. S.: Newton-Krylov-multigrid solvers for large-scale, highly heterogeneous, variably saturated flow problems, Adv. Water Resour., 24(7), 763–774, doi:10.1016/S0309-1708(00)00075-0, 2001.

Keune, J., Gasper, F., Goergen, K., Hense, A., Shrestha, P., Sulis, M., and Kollet, S.: Studying the influence of groundwater representations on land surface-atmosphere feedbacks during the European heat wave in 2003, J. Geophys. Res., 121(22), 13,301-13,325, doi:10.1002/2016JD025426, 2016.

Khorsandi, E., Kollet, S., Venema, V., and Simmer, C.: Investigating the effect of bottom boundary condition placement on ground heat storage in climate time scale simulations using ParflowE, Geophys. Res., 16(4), 2014, doi:10.1029/2006GL028546, 2014.

Kirkner, D. J., and Reeves, H.: Multicomponent Mass Transport With Homogeneous and Heterogeneous Chemical Reactions' Effect of the Chemistry on the Choice of Numerical Algorithm 1. Theory, Water Resour. Res., 24(10), 1719–1729, 1988.

Koch, J., Cornelissen, T., Fang, Z., Bogena, H., Diekkrüger, B., Kollet, S., and Stisen, S.: Inter-comparison of three distributed hydrological models with respect to seasonal variability of soil moisture patterns at a small forested catchment, *J. Hydrol.*, *533*, 234–249, doi:10.1016/j.jhydrol.2015.12.002, 2016.

Kollet, S., Sulis, M., Maxwell, R. M., Paniconi, C., Putti, M., Bertoldi, G., Coon, E. T., Cordano, E., Endrizzi, S., Kikinzon, E., Mouche, E., Mugler, C., Young-Jin Park, J. C. Refsgaard, Stisen Simo, and E. S.: The integrated hydrologic model intercomparison project,IH-MIP2: A second set of benchmark results to diagnoseintegrated hydrology and feedbacks, Water Resour. Res., 52(1), 1–20, doi:10.1002/2014WR015716, 2017.

Kollet, S. J.: Influence of soil heterogeneity on evapotranspiration under shallow water table conditions: transient, stochastic simulations, Environ. Res. Lett., 4, 035007, doi:10.1088/1748-9326/4/3/035007, 2009.

Kollet, S. J.: Optimality and inference in hydrology from entropy production considerations: synthetic hillslope numerical experiments., Hydrol. Earth Syst. Sci., 12, 5123–5149, 2015.

Kollet, S. J., and Maxwell, R. M.: Integrated surface-groundwater flow modeling: A free-surface overland flow boundary condition in a parallel groundwater flow model, Adv. Water Resour., 29(7), 945–958, doi:10.1016/j.advwatres.2005.08.006, 2006.

Kollet, S. J., and Maxwell, R. M.: Capturing the influence of groundwater dynamics on land surface processes using an integrated, distributed watershed model, Water Resour. Res., 44(2), 1–18, doi:10.1029/2007WR006004, 2008a.

Kollet, S. J., and Maxwell, R. M.: Demonstrating fractal scaling of baseflow residence time distributions using a fully-coupled groundwater and land surface model, Geophys. Res. Lett., 35(7), 1–6, doi:10.1029/2008GL033215, 2008b.

Kollet, S. J., Cvijanovic, I., Schüttemeyer, D., Maxwell, R. M., Moene, A. F., and Bayer, P.: The Influence of Rain Sensible Heat and Subsurface Energy Transport on the Energy Balance at the Land Surface, Vadose Zo. J., 8(4), 846, doi:10.2136/vzj2009.0005, 2009.

Kollet, S. J., Maxwell, R. M., Woodward, C. S., Smith, S., Vanderborght, J., Vereecken, H., and Simmer, C.: Proof of concept of regional scale hydrologic simulations at hydrologic resolution utilizing massively parallel computer resources, Water Resour. Res., 46(4), 1–7, doi:10.1029/2009WR008730, 2010.

Kumar, M., Duffy, C. J., and Salvage, K. M.: A second-order accurate, finite volume–based, integrated hydrologic modeling (FIHM) framework for simulation of surface and subsurface flow, Vadose Zo. J., 8(4), 873, doi:10.2136/vzj2009.0014, 2009.

LaBolle, E. M., Ahmed, A. A., and Fogg, G. E.: Review of the Integrated Groundwater and Surface-Water Model (IGSM), Ground Water, 41(2), 238–246, doi:10.1111/j.1745-6584.2003.tb02587.x, 2003.

Levis, S., and Jaeger, E. B.: COSMO-CLM2 : a new version of the COSMO- CLM model coupled to the Community Land Model coupled to the Community Land Model, Clim. Dyn., 37(November), 1889–1907, doi:10.1007/s00382-011-1019-z, 2011.

Li, L., Steefel, C. I., Kowalsky, M. B., Englert, A., and Hubbard, S. S.: Effects of physical and geochemical heterogeneities on mineral transformation and biomass accumulation during uranium bioremediation at Rifle, Colorado, J. Contam. Hydrol., 11, 45–63, 2010.

Li, L., Steefel, C. I., and Yang, L.: Scale dependence of mineral dissolution rates within single pores and fractures, Geochim. Cosmochim. Acta, 72, 360–377, doi:10.1016/j.gca.2007.10.027, 2007.

Markstrom, S. L., Niswonger, R. G., Regan, R. S., Prudic, D. E., and Barlow, P. M.: GSFLOW—Coupled Ground-Water and Surface-Water Flow Model Based on the Integration of the Precipitation-Runoff Modeling System (PRMS) and the Modular Ground-Water Flow Model (MODFLOW-2005), U.S. Geol. Surv., (Techniques and Methods 6-D1), 240, 2008.

Maxwell, R. M., and Miller, N. L.: Development of a Coupled Land Surface and Groundwater Model, J. Hydrometeorol., 6, 233–247, doi:10.1175/JHM422.1, 2005.

Maxwell, R. M.: Infiltration in Arid Environments: Spatial Patterns between Subsurface Heterogeneity and Water-Energy Balances, Vadose Zo. J., 9(4), 970, doi:10.2136/vzj2010.0014, 2010.

Maxwell, R. M.: A terrain-following grid transform and preconditioner for parallel, large-scale, integrated hydrologic modeling, Adv. Water Resour., 53, 109–117, doi:10.1016/j.advwatres.2012.10.001, 2013.

Maxwell, R. M., Welty, C., and Tompson, A. F. B.: Streamline-based simulation of virus transport resulting from long term artificial recharge in a heterogeneous aquifer, Adv. Water Resour., 26(10), 1075–1096, doi:10.1016/S0309-1708(03)00074-5, 2003.

Maxwell, R. M., Chow, F. K., and Kollet, S. J.: The groundwater–land-surface–atmosphere connection: Soil moisture effects on the atmospheric boundary layer in fully-coupled simulations, Adv. Water Resour., 30(12), 2447–2466, doi:10.1016/j.advwatres.2007.05.018, 2007.

Maxwell, R. M., Lundquist, J. K., Mirocha, J. D., Smith, S. G., Woodward, C. S., and Tompson, A. F. B.: Development of a Coupled Groundwater–Atmosphere Model, Mon. Weather Rev., 139(1), 96–116, doi:10.1175/2010MWR3392.1, 2011.

Maxwell, R. M., Condon, L. E., and Kollet, S. J.: A high-resolution simulation of groundwater and surface water over most of the continental US with the integrated hydrologic model ParFlow v3, Geosci. Model Dev, 923–937, doi:10.5194/gmd-8-923-2015, 2015.

Maxwell, R. M. et al.: Surface-subsurface model intercomparison: A first set of benchmark results to diagnose integrated hydrology and feedbacks, Water Resour. Res., 50, 1531–1549, doi:10.1002/2013WR013725, 2014.

Maxwell, R. M. et al.: ParFlow User 's Manual, 2016.

Meehl, G. A., Covey, C., McAvaney, B., Latif, M., and Stouffer, R. J.: Overview of the coupled model intercomparison project, Bull. Am. Meteorol. Soc., 86(1), 89–93, doi:10.1175/BAMS-86-1-89, 2005.

Meyerhoff, S. B., and Maxwell, R. M.: Using an integrated surface-subsurface model to simulate

runoff from heterogeneous hillslopes, in xviii International Conference on Water Resources, CIMNE, Barcelona, 2010.

Michalakes, J., Dudhia, J., Gill, D., Klemp, J., and Skamarock, W.: Design of a next-generation regional weather research and forecast model, Towar. Teracomputing, 19999.

Michalakes, J., Chen, S., Dudhia, J., Hart, L., Klemp, J., Middlecoff, J., and Skamarock, W.: Development of a next-generation regional weather research and forecast model, Towar. Teracomputing, 2001.

Mikkelson, K. M., Maxwell, R. M., Ferguson, I., Stednick, J. D., Mccray, J. E., and Sharp, J. O.: Mountain pine beetle infestation impacts: Modeling water and energy budgets at the hill-slope scale, Ecohydrology, 6(1), 64–72, doi:10.1002/eco.278, 2013.

Mironov, D., Heise, E., Kourzeneva, E. and Ritter, B.: Implementation of the lake parameterisation scheme FLake into the numerical weather prediction model COSMO, Boreal Environ. Res., 6095(April), 218–230, 2010.

Mobley, C. D., and Stewart, R. S.: On the numerical generation of boundary-fitted orthogonal curvilinear coordinate systems, J. Comput. Phys., 34(1), 124–135, doi:10.1016/0021-9991(80)90117-5, 1980.

Molders, N., and Ruhaak, W.: On the impact of explicitly predicted runoff on the simulated atmospheric response to small-scale land-use changes—an integrated modeling approach, Atmos. Res., 63, 2002.

Navarre-Sitchler, A., Steefel, C. I., Sak, P. B., and Brantley, S. L.: A reactive-transport model for weathering rind formation on basalt, Geochim. Cosmochim. Acta, 75, 7644–7667, doi:10.1016/j.gca.2011.09.033, 2011.

Oleson, K. W. et al.: Improvements to the Community Land Model and their impact on the hydrological cycle, J. Geophys. Res. Biogeosciences, 113(G1), doi:10.1029/2007JG000563, 2008.

Osei-Kuffuor, D., Maxwell, R. M., and Woodward, C. S.: Improved numerical solvers for implicit coupling of subsurface and overland flow, Adv. Water Resour., 74, doi:10.1016/j.advwatres.2014.09.006, 2014.

Panday, S., and Huyakorn, P. S.: A fully coupled physically-based spatially-distributed model for evaluating surface/subsurface flow, Adv. Water Resour., 27(4), 361–382, doi:10.1016/j.advwatres.2004.02.016, 2004.

Rahman, M., Sulis, M., and Kollet, S. J.: Evaluating the dual-boundary forcing concept in subsurface-land surface interactions of the hydrological cycle, Hydrol. Process., 30(10), 1563–1573, doi:10.1002/hyp.10702, 2016.

Ren, D., and Xue, M.: A revised force–restore model for land surface modeling, Am. Meteorol. Soc, 2004.

Reyes, B., Maxwell, R. M,. and Hogue, T. S.: Impact of lateral flow and spatial scaling on the simulation of semi-arid urban land surfaces in an integrated hydrologic and land surface model, Hydrol. Process., 30(8), 1192–1207, doi:10.1002/hyp.10683, 2016.

Richards, L. A.: Capillary conduction of liquids through porous mediums, J. Appl. Phys., 1(5), 318–333, doi:10.1063/1.1745010, 1931.

Rigon, R., Bertoldi, G., and Over, T. M.: GEOtop: A Distributed Hydrological Model with Coupled Water and Energy Budgets, J. Hydrometeorol., 7(3), 371–388, doi:10.1175/jhm497.1, 2006.

Rihani, J.,F., Chow, F. K., Fotini K., and Maxwell, R. M.: Isolating effects of terrain and soil moisture heterogeneity on the atmospheric boundary layer: Idealized simulations to

diagnose land-atmosphere feedbacks, J. Adv. Model. Earth Syst., 6, 513–526, doi:10.1002/2014MS000371.Received, 2015.

Rihani, J. F., Maxwell, M. R., and Chow, F. K.: Coupling groundwater and land surface processes: Idealized simulations to identify effects of terrain and subsurface heterogeneity on land surface energy fluxes, Water Resour. Res., 46(12), 1–14, doi:10.1029/2010WR009111, 2010.

Ryskin, G., and Leal, L.: Orthogonal mapping, J. Comput. Phys., 50(1), 71–100, doi:10.1016/0021-9991(83)90042-6, 1983.

Saad, Y., and Schultz, M. H.: GMRES: A Generalized Minimal Residual Algorithm for Solving Nonsymmetric Linear Systems, SIAM J. Sci. Stat. Comput., 7(3), 856–869, doi:10.1137/0907058, 1986.

Seck, A., Welty, C., and Maxwell, R. M.: Spin-up behavior and effects of initial conditions for an integrated hydrologicmodel Alimatou, Water Resour. Res., 51, 2188–2210, doi:10.1002/2014WR016371.Received, 2015.

Seuffert, G., Gross, P., Simmer, A. C., and Wood, E. F.: The Influence of Hydrologic Modeling on the Predicted Local Weather: Two-Way Coupling of a Mesoscale Weather Prediction Model and a Land Surface Hydrologic Model, J. Hydrometeorol., 3, 2002.

Shen, C., and Phanikumar, M. S.: A process-based, distributed hydrologic model based on a large-scale method for surface-subsurface coupling, Adv. Water Resour., 33(12), 1524–1541, doi:10.1016/j.advwatres.2010.09.002, 2010.

Shi, Y., Davis, K. J., Zhang, F., and Duffy, C. J.: Evaluation of the Parameter Sensitivities of a Coupled Land Surface Hydrologic Model at a Critical Zone Observatory, J. Hydrometeorol., 15(1), 279–299, doi:10.1175/JHM-D-12-0177.1, 2014.

Shrestha, P., Sulis, M., Masbou, M., Kollet, S., and Simmer, C.: A Scale-Consistent Terrestrial Systems Modeling Platform Based on COSMO, CLM, and ParFlow, Mon. Weather Rev., 142, doi:10.1175/MWR-D-14-00029.1, 2014.

Shrestha, P., Sulis, M., Simmer, C., and Kollet, S.: Impacts of grid resolution on surface energy fluxes simulated with an integrated surface-groundwater flow model, Hydrol. Earth Syst. Sci, 19, 4317–4326, doi:10.5194/hess-19-4317-2015, 2015.

Simmer, C. et al.: Monitoring and modeling the terrestrial system from pores to catchments: The transregional collaborative research center on patterns in the soil-vegetation-atmosphere system, Bull. Am. Meteorol. Soc., 96(10), 1765–1787, doi:10.1175/BAMS-D-13-00134.1, 2015.

Skamarock, W. C., and Klemp, J. B.: A Time-Split Nonhydrostatic AtmosphericModel forWeather Research and Forecasting Applications, , (001), 1–43, 2007.

Skamarock, W. C., Klemp, J. B., Dudhia, J., Gill, D. O., Barker, D. M., Wang, W., and Powers, J. G.: A description of the advanced research WRF Version 2, 2005.

Smith, S. G., Ashby, S. F., Falgout, R. D., and Tompsom, A. F. B.: The parallel performance of a groundwater flow code on the CRAY T3D. In Proceedings of the Seventh SIAM Conference on Parallel Processing for Scientific Computing, 131, 1995.

Srivastava, V., Graham, W., Muñoz-Carpena, R., and Maxwell, R. M.: Insights on geologic and vegetative controls over hydrologic behavior of a large complex basin – Global Sensitivity Analysis of an integrated parallel hydrologic model, J. Hydrol., 519, 2238–2257, doi:10.1016/J. Hydrol.2014.10.020, 2014.

Steefel, C. I., and Yabusaki, S. B.: OS3D/GIMRT software for modeling multicomponent-multidimensional reactive transport, Richland, WA, 1996.

Steefel, C. I.: CrunchFlow Software for Modeling Multicomponent Reactive Flow and Transport User's Manual, 2009.

Steefel, C. I., and Van Cappellen, P.: A new kinetic approach to modeling water-rock interaction: The role of nucleation, precursors, and Ostwald ripening, Geochim. Cosmochim. Acta, 54(10), 2657–2677, doi:10.1016/0016-7037(90)90003-4, 1990.

Steefel, C. I., and Lasaga, A. C.: A coupled model for transport of multiple chemical species and kinetic precipitation/dissolution reactions with application to reactive flow in single phase hydrothermal systems, Am. J. Sci., 294(5), 529–592, doi:10.2475/ajs.294.5.529, 1994.

Steefel, C. I. et al.: Reactive transport codes for subsurface environmental simulation, Comput. Geosci., 19(3), 445–478, doi:10.1007/s10596-014-9443-x, 2015.

Steiner, A. L., Pal, J. S., Giorgi, F., Dickinson, R. E., and Chameides, W. L.: The coupling of the Common Land Model (CLM0) to a regional climate model (RegCM), Theor. Appl. Climatol., 82(3–4), 225–243, doi:10.1007/s00704-005-0132-5, 2005.

Steiner, A. L., Pal, J. S., Rauscher, S. A., Bell, J. L., Diffenbaugh, N. S., Boone, A., Sloan, L. C., and Giorgi, F.: Land surface coupling in regional climate simulations of the West African monsoon, Clim. Dyn., 33(6), 869–892, doi:10.1007/s00382-009-0543-6, 2009.

Sudicky, E. A., Jones, J. P., Park, Y. J., Brookfield, A. E., and Colautti, D.: Simulating complex flow and transport dynamics in an integrated surface-subsurface modeling framework, Geosci. J., 12(2), 107–122, doi:10.1007/s12303-008-0013-x, 2008.

Sulis, M., Meyerhoff, S. B., Paniconi, C., Maxwell, R. M., Putti, M., and Kollet, S. J.: A comparison of two physics-based numerical models for simulating surface water-groundwater interactions, Adv. Water Resour., 33(4), 456–467, doi:10.1016/j.advwatres.2010.01.010, 2010.

Sulis, M., Williams, J. L., Shrestha, P., Diederich, M., Simmer, C., Kollet, S. J., and. Maxwell, R. M.: Coupling Groundwater, Vegetation, and Atmospheric Processes: A Comparison of Two Integrated Models, J. Hydrometeorol., 18(5), 1489–1511, doi:10.1175/JHM-D-16-0159.1, 2017.

Therrien, R and Sudicky, E.: Three-dimensional analysis of variably-saturated flow and solute transport in discretely- fractured porous media, J. Contam. Hydrol., 23(95), 1–44, doi:10.1016/0169-7722(95)00088-7, 1996.

Tompson, A. F. B., Ababou, R., and Gelhar, L. W.: Implementation of the three-dimensional turning bands random field generator, Water Resour. Res., 25(10), 2227–2243, doi:10.1029/WR025i010p02227, 1989.

Tompson, A. F. B., Ashby, S. F., and Falgout, R. D.: Use of high performance computing to examine the effectiveness of aquifer remediation, 1994.

Tompson, A. F. B., Falgout, R. D., Smith, S. G., Bosl, W. J., and Ashby, S. F.: Analysis of subsurface contaminant migration and remediation using high performance computing, Adv. Water Resour., 22(3), 203–221, doi:10.1016/S0309-1708(98)00013-X, 1998.

Tompson, A. F. B., Carle, S. F., Rosenberg, N. D., and Maxwell, R. M.: Analysis of groundwater migration from artificial recharge in a large urban aquifer: A simulation perspective, Water Resour. Res., 35(10), 2981–2998, doi:10.1029/1999WR900175, 1999.

Valcke, S.: The OASIS3 coupler : a European climate modelling community software, Geosci. Model Dev, 6, 373–388, doi:10.5194/gmd-6-373-2013, 2013.

Valcke, S., Balaji, V., Bentley, P., Guilyardi, E., Lawrence, B., and Pascoe, C.: Developing a Common Information Model for climate models and data, Geophys. Res. Abstr., 11, 10592, 2009.

Valcke, S., Balaji, V., Craig, A., Deluca, C., Dunlap, R., Ford, R. W., Jacob, R., Larson, J., and Kuinghttons, O. R.: Model Development Coupling technologies for Earth System Modelling, Geosci. Model Dev., 5, 1589–1596, doi:10.5194/gmd-5-1589-2012, 2012.

VanderKwaak, J. E.: Numerical simulation of flow and chemical transport in integrated surface-subsurface hydrologic systems, 1999.

VanGenuchten, M. T.: A Closed-form Equation for Predicting the Hydraulic Conductivity of Unsaturated Soils, Soil Sci. Soc. Am. J., 44, 892–898, doi:10.2136/sssaj1980.03615995004400050002x, 1980.

Visbal, M., and Knight, D.: Generation of orthogonal and nearly orthogonal coordinates with gridcontrol near boundaries, AIAA J., 20(3), 305–306, doi:10.2514/3.7915, 1982.

Vogel, B., Vogel, H., Bangert, M., Lundgren, K., Rinke, R., and Stanelle, T.: The comprehensive model system COSMO-ART – Radiative impact of aerosol on the state of the atmosphere on the regional scale, Atmos. Chem. Phys., 9, 8661–8680, 2009.

Volker, J.: Multigrid Methods, , doi:10.1137/1.9781611971057, 1987.

Wagner, S., Fersch, B., Yuan, Y.,Yu, Z., and Kunstmann, H.: Fully coupled atmospheric-hydrological modeling at regional and long-term scales: Development, application, and analysis of WRF-HMS, Water Resour. Res., 52(4), 3187–3211, doi:10.1002/2015WR018185, 2016.

Weill, S., Mouche, E., and Patin, J.: A generalized Richards equation for surface/subsurface flow modelling, J. Hydrol., 366(1–4), 9–20, doi:10.1016/j.jhydrol.2008.12.007, 2009.

Weill, S., Mazzia, A., Putti, M., and Paniconi, C.: Coupling water flow and solute transport into a physically-based surface-subsurface hydrological model, Adv. Water Resour., 34(1), 128–136, doi:10.1016/j.advwatres.2010.10.001, 2011.

Williams, J. L., and Maxwell, R. M.: Propagating Subsurface Uncertainty to the Atmosphere Using Fully Coupled Stochastic Simulations, J. Hydrometeorol., 12(1994), 690–701, doi:10.1175/2011JHM1363.1, 2011.

Williams, J. L., Maxwell, R. M., and Monache, L. D.: Development and verification of a new wind speed forecasting system using an ensemble Kalman filter data assimilation technique in a fully coupled hydrologic and atmospheric model, J. Adv. Model. Earth Syst., 5(4), 785–800, doi:10.1002/jame.20051, 2013.

Wood, B. D.: The role of scaling laws in upscaling, Adv. Water Resour., 32(5), 723–736, doi:10.1016/j.advwatres.2008.08.015, 2009.

Woodward, S. C.: A Newton-Krylov-multigrid solver for variably saturated flow problems, Proceedings on the Twelfth International Conference on Computational Methods in Water Resources, in Computational Mechanics Publications, vol. 2, pp. 609–616, 1998.

Xu, L., Raman, S., and Madala, R. V.: A review of non-hydrostatic numerical models for the atmosphere, Math. Subj. Classif, 1991.

Xue, M., Droegemeier, K. K., and Wong, V.: The Advanced Regional Prediction System (ARPS) - A multi-scale nonhydrostatic atmospheric simulation and prediction tool. Part II: Model dynamics and verification, Meteorol. Atmos. Phys., 75, 161–193, doi:10.1007/s007030170027, 2000.

Zhufeng F., Bogena, H., Kollet, S., Koch, J. H. V.: Spatio-temporal validation of long-term 3D hydrological simulations of a forested catchment using empirical orthogonal functions and wavelet coherence analysis, Hydrology, 529(1754–1767), 2015.